

1 **Measurement report: Enhanced photochemical formation of**
2 **formic and isocyanic acids in urban region aloft: insights**
3 **from tower-based online gradient measurements**

4 Qing Yang^{1,2}, Xiao-Bing Li^{1,2,*}, Bin Yuan^{1,2,*}, Xiaoxiao Zhang^{1,2}, Yibo Huangfu^{1,2}, Lei
5 Yang^{1,2}, Xianjun He^{1,2}, Jipeng Qi^{1,2}, Min Shao^{1,2}

6 ¹ Institute for Environmental and Climate Research, Jinan University, Guangzhou
7 511443, China

8 ² Guangdong-Hongkong-Macau Joint Laboratory of Collaborative Innovation for
9 Environmental Quality, Guangzhou 511443, China

10 * Corresponding authors: Xiao-Bing Li (lixiaobing@jnu.edu.cn), Bin Yuan
11 (byuan@jnu.edu.cn)

12 **Abstract**

13 Formic acid is the most abundant organic acid in the troposphere and has
14 significant environmental and climatic impacts. Isocyanic acid poses severe threats to
15 human health and could be formed through the degradation of formic acid. However,
16 the lack of vertical observation information has strongly limited the understanding of
17 their sources, particularly in urban regions with complex pollutant emissions. To
18 address this issue, we assessed the impact of long tubes on the measurement
19 uncertainties of formic and isocyanic acids and found that the tubing impact was
20 negligible. Then, we conducted continuous (27 days) vertical gradient measurements
21 (five heights between 5-320 m) of formic and isocyanic acids using long tubes based
22 on a tall tower in Beijing, China, in the summer of 2021. Results show that the
23 respective mean mixing ratios of formic and isocyanic acids were 1.3 ± 1.3 ppbv and
24 0.28 ± 0.16 ppbv at 5 m and were 2.1 ± 1.9 ppbv and 0.43 ± 0.21 ppbv at 320 m during the
25 campaign. The mixing ratios of formic and isocyanic acids were substantially enhanced
26 in daytime and correlated with the diurnal change of ozone. Upon sunrise, the mixing
27 ratios of formic and isocyanic acids at different heights simultaneously increased even
28 in the residual layer. In addition, positive vertical gradients were observed for formic
29 and isocyanic acids throughout the day. The positive vertical gradients of formic and
30 isocyanic acids in daytime imply the enhancement of their secondary formation in
31 urban regions aloft, predominantly due to the enhancements of oxygenated volatile
32 organic compounds. Furthermore, the afternoon peaks and positive vertical gradients
33 of formic and isocyanic acids in nighttime also indicate their minor contributions from
34 primary emissions from ground-level sources. The formation pathway of isocyanic acid
35 through $\text{HCOOH}-\text{CH}_3\text{NO}-\text{HNCO}$ was enhanced with height but only accounted for a
36 tiny fraction of its ambient abundance. The abundance and source contributions of
37 formic and isocyanic acids in the atmospheric boundary layer may be highly
38 underestimated when being derived from their ground-level measurements. With the
39 aid of numerical modeling techniques, future studies could further identify key

40 precursors that drive the rapid formation of formic and isocyanic acids, and
41 quantitatively assess the impacts of the enhanced formation of the two acids aloft on
42 their budgets at ground level.

43 **1. Introduction**

44 Formic acid (HCOOH) is the simplest but the most abundant organic acid in the
45 troposphere. It has been widely measured in aqueous (clouds and aerosols) and gaseous
46 phases over urban, rural, and remote regions (*Kawamura and Kaplan, 1983; Chebbi
47 and Carlier, 1996; Kesselmeier et al., 1998; Yu, 2000*). As important contributors to the
48 acidity of precipitation, formic and acetic acids can account for 60% of the free acidity
49 in remote regions (*Galloway et al., 1982; Andreae et al., 1988*), and over 30% of the
50 free acidity in heavily polluted regions (*Keene and Galloway, 1984*). Formic acid is
51 also an important sink of hydroxyl radicals (OH) in clouds (*Jacob, 1986*), playing vital
52 roles in modulating the atmospheric aqueous-phase chemistry through changing pH-
53 dependent reaction rates of related constituents. An in-depth understanding of the
54 concentration levels, spatiotemporal variations, and sources of formic acid is key to
55 elucidating the formation mechanisms of atmospheric secondary pollution. However,
56 the sources and sinks of atmospheric formic acid are still poorly understood so far.

57 There have been many reported sources of atmospheric formic acid. Primary
58 emissions from vegetation activity (*Andreae et al., 1988; Kesselmeier et al., 1998*),
59 microbial metabolism (*Enders et al., 1992*), biomass burning (*Goode et al., 2000*), and
60 vehicle exhaust (*Kawamura et al., 2000*) were identified as important sources of formic
61 acid. Secondary formation from photochemical degradation of volatile organic
62 compounds (VOCs) is another significant source of formic acid (*Khare et al., 1999;
63 Veres et al., 2011; Le Breton et al., 2014; Liggiio et al., 2017*). However, current
64 chemical transport models still highly underestimate ambient concentrations of formic
65 acid (*Stavrakou et al., 2011; Paulot et al., 2011; Millet et al., 2015*) and cannot well
66 reproduce its vertical variations. For example, Mattila et al. (2018) measured vertical
67 profiles of formic acid using an elevator on the Colorado Front Range BOA tower. They
68 found that formic acid mixing ratios generally decreased with height throughout the day,
69 but there were no known sources to explicitly explain the net surface emissions. In
70 combination with vertical gradient and flux measurements of formic acid in a forest

71 ecosystem, Alwe et al. (2019) suggested that secondary formation, rather than primary
72 emission, is the major source of ambient formic acid. The vertical distribution and
73 variation patterns of formic acid in the atmospheric boundary layer can provide
74 valuable information on the identification and determination of source contributions.
75 Nevertheless, the vertical variations and key drivers of formic acid, particularly in urban
76 regions, are still unclear due to the lack of adequate vertical observations.

77 Isocyanic acid (HNCO) is an inorganic acid and has attracted extensive concerns
78 worldwide in recent years due to its strong toxicity (Wang et al., 2007; Jaisson et al.,
79 2011; Koeth et al., 2013). Previous studies have reported that isocyanic acid is highly
80 soluble at physiological pH and the dissociated cyanate ions (NCO^-) are closely linked
81 to atherosclerosis, cataracts, and rheumatoid arthritis (Mydel et al., 2010; Roberts et al.,
82 2011). At present, there is no standard to clearly define the critical levels of isocyanic
83 acid pollution in ambient air (Rosanka et al., 2020). The mixing ratio of HNCO in the
84 atmosphere exceeding 1 ppbv may endanger human health (Roberts et al., 2011), and
85 the protein carbamylation caused by HNCO in human body may induce various risks
86 (Verbrugge et al., 2015). Similar to formic acid, our understanding of isocyanic acid
87 sources is also very limited.

88 As reported in the literature, primary emissions of isocyanic acid are mainly from
89 combustion sources including cigarette smoke (Hems et al., 2019), gasoline and diesel
90 engine exhausts (Wren et al., 2018), and biomass combustion (Wentzell et al., 2013; Li
91 et al., 2021; Chandra and Sinha, 2016). Wet and dry deposition is known as the main
92 sink of isocyanic acid (Roberts et al., 2014; Rosanka et al., 2020). In addition, isocyanic
93 acid is highly soluble at atmospheric pH and can be hydrolyzed to NH_3 and CO_2 (Zhao
94 et al., 2014; Roberts and Liu, 2019). Secondary formation is another important source
95 of atmospheric isocyanic acid and the known precursors include amides (Barnes et al.,
96 2010), urea (Jathar et al., 2017), and nicotine (Roberts et al., 2011; Borduas et al.,
97 2016). Amides are reported to be the main precursors of isocyanic acid in urban regions
98 (Wang et al., 2020). Isocyanic acid is the oxidative degradation product of amides

99 initiated by OH radicals, NO₃, radicals, and Cl atoms (*Barnes et al., 2010*). In addition
100 to primary emissions from organic solvents and various industrial processes, amides
101 can be also formed through the atmospheric accretion reactions of organic acids with
102 amines or ammonia (*Barnes et al., 2010; Yao et al., 2016*). Vertical gradient
103 measurements of HNCO can help elucidate potential formation sources and
104 mechanisms.

105 Chemical ionization mass spectrometry (CIMS) can effectively detect and
106 quantify atmospheric formic and isocyanic acids (*Bannan et al., 2014; Chandra and*
107 *Sinha, 2016; Liggio et al., 2017; Mungall et al., 2018; Fulgham et al., 2019*). CIMS
108 has been widely used onboard aircraft or on towers to make online vertical
109 measurements of formic and isocyanic acids (*Liggio et al., 2017; Mattila et al., 2018*).
110 Aircraft can carry many types of instruments and achieve measurements of a large suite
111 of parameters (*Benish et al., 2020; Zhao et al., 2021*), but the cost is also very expensive.
112 Towers can provide vertical observations of target species by setting up sites at different
113 heights, building mobile platforms (elevators or baskets) (*Mattila et al., 2018*), and
114 drawing air from multiple heights to the ground-based instruments through long tubes
115 (*Hu et al., 2013; Yáñez-Serrano et al., 2018*). The usage of long tubes is the most
116 convenient and cost-effective method to make gradient measurements of target gaseous
117 species so far. However, interactions between gaseous species and tubing walls may
118 bring unexpected uncertainties for their measurements (*Helmig et al., 2008a; Helmig*
119 *et al., 2008b; Schnitzhofer et al., 2009; Karion et al., 2010; Pagonis et al., 2017*).
120 Therefore, the impacts of long tubing on measurements of formic and isocyanic acids
121 need to be elucidated.

122 In this study, we first assessed the effects of long perfluoroalkoxy (PFA) Teflon
123 tubes on measurements of formic and isocyanic acids. Vertical gradient measurements
124 of the two acids were made through long tubes on a tall tower in urban Beijing, China.
125 Then, the vertical variations and sources of the two acids were investigated and
126 discussed. At last, key conclusions and implications of this study were summarized.

127 **2. Methods and materials**

128 **2.1. Site description and field campaign**

129 Vertical gradient measurements of gaseous species were made on the Beijing
130 Meteorological Tower, which is located on the campus of the Institute of Atmospheric
131 Physics (IAP), Chinese Academy of Sciences. Beijing is the capital city of China with
132 a population of over 20 million by 2020. Beijing has large anthropogenic emission
133 intensities and is suffering from severe air pollution problems (*Acton et al., 2020; Meng*
134 *et al., 2020; Tan et al., 2022*). The tower is located in the northern part of downtown
135 Beijing between the 3rd and 4th Ring Roads and is surrounded by urban roads,
136 expressways, residential areas, restaurants, urban landscaping, and parks. As a result,
137 concentrations of the primary pollutants at the tower site are mainly contributed by both
138 anthropogenic (e.g., vehicular exhausts, cooking, and household volatile chemical
139 products) and biogenic emissions. Detailed descriptions of the tower have been
140 provided in previous studies (*Acton et al., 2020; Yan et al., 2021*) and will not be
141 repeated here. The field campaign was carried out from July 17th to August 3rd, 2021.

142 **2.2. Instrumentation**

143 To obtain online gradient measurements of atmospheric trace gases, we
144 established a tower-based observation system using a combination of online
145 measurement techniques and long tubes (Figure S1). The system and related
146 assessments on the usage of long tubes have been explicitly described in our previous
147 study (*Li et al., 2023*) and will be briefly introduced here. After removing fine particles
148 by PFA Teflon filters (Whatman) with a diameter of 46.2 mm and a pore size of 2 μm ,
149 ambient air at four altitudes on the tower (namely 47, 102, 200, and 320 m) was
150 simultaneously and continuously drawn to the ground through long PFA Teflon tubes
151 (100, 150, 250, and 400 m; outer diameter: 1/2"; inner diameter: 0.374") by a vacuum
152 pump. All the sampling tubes were installed inside the iron tower to avoid direct
153 sunlight. The flow rate of the sample stream in each tube was controlled by a critical

154 orifice and ranged between 13-21 standard liters per minute (SLPM), as shown in table
155 S1. The flow rates in long tubes were retained as large as possible if instruments allowed
156 to minimize the impact of gas-surface interactions on measurements of targeted gaseous
157 species (*Deming et al., 2019; Li et al., 2023*). Two air-conditioned containers were
158 placed next to each other on the base of the tower and all the instruments were operated
159 inside. An additional inlet of the tube was mounted on the rooftop of the container
160 (approximately 5 m above ground level) to make measurements of trace gases near the
161 surface. Therefore, the tower-based observation system consisted of five inlet heights
162 ranging from the ground level to 320 m. Inlets of the instruments were connected to the
163 outlet of a Teflon solenoid valve group, which was used to perform the switch of the
164 inlet heights at time intervals of 4 minutes. Vertical gradient measurements of gaseous
165 species were cyclically made over periods of 20 minutes. Indoor PFA Teflon tubes were
166 wrapped with insulation tubes and were heated to prevent condensation of water and
167 organic gases.

168 Formic and isocyanic acids were measured by a high-resolution time-of-flight
169 chemical ionization mass spectrometry with iodide reagent ion (ToF-CIMS). Due to the
170 high sensitivity to oxygenated volatile organic compounds (OVOCs), the iodine ion
171 source has been widely used in previous studies (*Yuan et al., 2015; Schobesberger et*
172 *al., 2016; Mungall et al., 2018*). A Filter Inlet for Gases and AEROSols (FIGAERO)
173 was used to perform the switch between the gas and particle measurement modes
174 (*Lopez-Hilfiker et al., 2014*). The ion molecular reaction (IMR) chamber is adjacent to
175 the FIGAERO and utilizes a vacuum ultraviolet ion source (VUV-IS). Iodide anion (I^-)
176 is produced from the photoionization of methyl iodide (CH_3I) in IMR (*Ji et al., 2020*).
177 During the measurements, I^- was produced by introducing the CH_3I gas standard (1000
178 ppm, Dalian Special Gases, China) to the IMR chamber at a flow rate of 2 standard
179 cubic centimeters per minute (SCCM) in 200 SCCM high-purity nitrogen (N_2 ,
180 99.9995%) by the VUV-IS. The pressure of the IMR chamber was maintained at 70-80
181 mbar. Flow rates of the sample gas were maintained at 2 SLPM using a critical orifice.

182 During the field campaign, both gaseous and particle measurements were made through
183 the FIGAERO of the CIMS, but only gaseous measurements were analyzed in this study.
184 In a one-hour cycle, the first 24 min was allocated to make gaseous measurements
185 during which a complete vertical profile of a gaseous species can be obtained. As shown
186 in Figure S3, there was no significant difference between the background signals of the
187 instrument made with and without the long tubes. Therefore, blank measurements of
188 the instrument were made by adding zero air just to the inlet of the instrument without
189 through the long tubes during the field campaign. In the gaseous measurement mode, a
190 rapid blank measurement was made for 10 s at 3-min intervals in the first 21 min and a
191 long-time blank measurement was made in the rest 3 min (*Palm et al., 2019*). During
192 the first 21-min period of the one-hour cycle, another inlet at 5 m was used to collect
193 ambient particles using PTFE membrane filters (Zefluor®, Pall Inc., USA). Therefore,
194 the remaining 36 min of the one-hour cycle was allocated to analyze the collected
195 particle.

196 Calibrations of the ToF-CIMS for formic and isocyanic acids were performed in
197 the laboratory before and after the field campaign. Standard solutions of formic acid
198 were evaporated using the liquid calibration unit (LCU, IONICON Analytik GmbH)
199 and then diluted to designated concentration gradients by being mixed with zero air at
200 five flow rates. The gas standard of isocyanic acid is unstable at ambient temperature
201 and thus no commercial gas cylinder was available. Instead, cyanuric acid solution was
202 put into a diffusion cell and heated to 300 °C to generate isocyanic acid gas at a stable
203 mixing ratio. An ion chromatograph was used to quantify the concentration of the gas
204 standard by measuring deionized water that absorbed the isocyanic acid gas. Detailed
205 information about the isocyanic acid calibration procedure has been provided in our
206 previous work (*Wang et al., 2020*). Impacts of the changes in ambient humidity on
207 measurements of the ToF-CIMS for both formic and isocyanic acids were determined
208 in the laboratory and were corrected when calculating their respective concentrations.
209 Measured signals of the ToF-CIMS were processed using the Tofware software package

210 (version 3.0.3; ToFwerk AG, Switzerland).

211 A high-resolution proton-transfer-reaction quadrupole interface time-of-flight
212 mass spectrometry (PTR-ToF-MS) with both H_3O^+ and NO^+ ion chemistry was used to
213 measure reported precursors of the two acids, such as isoprene, aromatics, OVOCs, and
214 amides. Detailed information about the configuration and operation setup of the PTR-
215 ToF-MS has been provided in our previous studies (*Yuan et al., 2017; Wu et al., 2020;*
216 *Li et al., 2022*). Mixing ratios of O_3 , CO, and NO_2 were measured by a UV absorption
217 O_3 analyzer (T400, Teledyne API, USA), a gas filter correlation CO analyzer (T300,
218 Teledyne API, USA), and a trace level NO_x analyzer (42i, Thermo, USA), respectively.
219 Photolysis rates were measured by a PFS-100 photolysis spectrometer (Focused
220 Photonics Inc.) on the rooftop of the container. The planetary boundary layer height
221 (PBLH) data was obtained from the web portal of the Real-time Environmental
222 Applications and Display sYstem (READY) of the National Oceanic and Atmospheric
223 Administration (NOAA) Air Resource Laboratory
224 (<https://ready.arl.noaa.gov/READYamet.php>). Measurements of isocyanic acid and
225 amides made in Guangzhou and Gucheng in China were also used in this study for
226 comparison, and more information about these observations can be found in our
227 previous papers (*Wang et al., 2020*).

228 **2.3. Tubing assessment**

229 The tower-based observation system used long PFA Teflon tubes (hundreds of
230 meters in length) to draw air samples from different heights. The interactions between
231 tubing inner walls and organic compounds, namely the absorption/desorption of trace
232 gases, have nonnegligible impacts on their measurements after traversing such long
233 tubes (*Pagonis et al., 2017; Deming et al., 2019*). The equilibrium between the
234 absorption and desorption of organic compounds on tubing walls required distinct times,
235 namely tubing delay, for different species. For nonpolar/weak-polar organic compounds,
236 their tubing delays and measurement uncertainties after traversing long tubes are
237 dependent on their saturation concentrations and the flow rates of sample streams but

238 are independent of changes in humidity (*Krechmer et al., 2017; Pagonis et al., 2017*).
239 For some small polar organic compounds, their tubing delays and measurement
240 uncertainties after traversing long tubes are dependent on Henry's law coefficients and
241 are affected by changes in humidity (*Liu et al., 2019*). The performance of long PFA
242 Teflon tubes in measuring concentrations of nonpolar/weak-polar organic compounds
243 and inorganic species (e.g., ozone, NO, NO₂, and CO₂) has been assessed in our
244 previous work (*Li et al., 2023*). The impacts of long PFA Teflon tubes on measurements
245 of formic and isocyanic acids are still unclear and will be assessed in this study.

246 Long PFA Teflon tubes with an outer diameter of 1/2" and an inner diameter of
247 0.374" were used to draw air samples from different altitudes and thus were assessed.
248 At flow rates below 20 SLPM, suitable pressure drops can be maintained in these long
249 tubes for instrument operation (*Li et al., 2023*). The effects of long tubes on
250 measurements of formic and isocyanic acids were mainly assessed using the same
251 methods in the literature (*Li et al., 2023*). The tubing delay of formic acid is estimated
252 as the time required to reach 90% of the concentration change made at the tubing inlet.
253 The depassivation curve of formic acid measured at the outlet end of the long tubing
254 was used to calculate its tubing delay and was obtained by using a step-function change
255 of the formic acid concentration from 7.5 ppbv to 0 ppbv at the tubing inlet (*Pagonis et*
256 *al., 2017; Deming et al., 2019*). The formic acid signals were normalized to those
257 measured at the beginning of the step-function change and then were fitted using the
258 double exponential method, as shown in Figure 1. Finally, the tubing delay of formic
259 acid was determined when the fitting line decreased to 0.1. The previous study (*Li et*
260 *al., 2023*) has reported that inorganic species have small tubing delays even in a 400 m
261 long tube. Therefore, tubing delays of isocyanic acid in long tubes are not discussed in
262 this study.

263 To further assess the impacts of long tubes (namely 100, 200, 300, and 400 m)
264 on measurements of formic and isocyanic acids in real environments, their ambient
265 mixing ratios measured through different lengths of tubes were intercompared by

266 running the inlets side by side at ground level. Ambient air samples were sequentially
267 drawn with and without the tubes through a Teflon solenoid valve group (Figure S2),
268 which was set to perform the switch at time intervals of 4 minutes. Instrument
269 backgrounds of the two species were measured for 10 s at time intervals of 1 minute by
270 passing zero air into the instrument at a flow rate of 3 SLPM. Inter-comparisons of the
271 formic acid and isocyanic acid measurements made through different lengths of tubes
272 were mainly performed using linear fittings ($y=kx+b$; k is the slope and b is the
273 intercept).

274 **3. Results and Discussions**

275 **3.1. Interactions between long tubes and the two acids**

276 As shown in Figure 1, signals of formic acid measured by the ToF-CIMS had a
277 tubing delay of 23 s after traversing the 400 m long tube at the flow rate of 13 SLPM.
278 In addition to the interactions between tubing walls and formic acid molecules (*Pagonis*
279 *et al.*, 2017; *Deming et al.*, 2019), molecular diffusion and dispersion (namely Taylor
280 dispersion) can cause the longitudinal mixing of gas molecules in the tubing and is also
281 an important factor contributing to the measured delays (*Karion et al.*, 2010). Molecular
282 diffusion and dispersion have strong dependences on molecular diffusion coefficients
283 and tubing flow rates (*Karion et al.*, 2010). The influential time of Taylor dispersion on
284 the measurements of formic acid through a 400 m long tube at the flow rate of 13 SLPM
285 was estimated to be only 2.9 s, which is much smaller than the measured tubing delay
286 (23 s) of formic acid. Therefore, the adsorption/desorption of formic acid molecules on
287 tubing inner walls plays a dominant role in determining the tubing delay.

288 For most organic compounds, the tubing delays generally depend on tubing flow
289 rates and their saturated concentrations (C^*) (*Li et al.*, 2023; *Deming et al.*, 2019). With
290 the increase in tubing length and flow rate, the tubing delays of organic compounds will
291 rapidly decrease (*Liu et al.*, 2019). Therefore, the tubing flow rates should be as large
292 as possible if the instrument could work normally. In addition, the tubing delays of

293 organic compounds generally increase with the decrease in their C^* (Li et al., 2023). It
294 must be acknowledged that tubing delay is inevitable. The analysis time scales of
295 species concentrations measured through long tubes should be greater than their tubing
296 delays, especially for those with small C^* .

297 The delay time of formic acid mentioned here is different from the residence time
298 of the gas through the long tubing. Residence time refers to the time required for the
299 sample gas to pass through the tubes. As for the measured tubing delays of trace gases,
300 they refer to the amounts of time required for the instruments to measure stable
301 concentrations of targeted species in response to a change in species concentrations at
302 the tubing inlet. The residence time is the same for all trace gases, depending on the
303 length of the long tube, the inner diameter of the tube, and the flow rate of the sample
304 gas. However, the tubing delay for each trace gas is different and depends on the flow
305 rate, their respective saturated concentrations/Henry's constants, and molecular
306 diffusion and diffusion rates. The difference between residence time and delay time is
307 also discussed in detail in our previous work (Li et al., 2023).

308 As shown in Figure S4(a), ambient mixing ratios of formic acid measured
309 through the 400 m long tube varied consistently with those measured without the tube
310 with mean values of 4.14 and 4.09 ppbv, respectively. The mixing ratios of formic acid
311 measured with the long tube were slightly higher in the daytime and lower at night in
312 comparison with those measured without the long tube. We also conducted a correlation
313 analysis between the mixing ratios of formic acid measured with and without long tubes.
314 As shown in Figure 2, the mixing ratios of formic acid measured with and without the
315 400 m long tube agreed within 20%, but the slope of the linear fitting ($k=0.84$) is lower
316 than 1. The differences of formic acid mixing ratios measured with and without the 400
317 m long tube were predominantly caused by the long-tail memory effect of the tubing
318 (Figure 1). For example, the mixing ratios of formic acid measured through the 400 m
319 long tube at night equaled to its ambient mixing ratios plus those released from the
320 tubing inner wall. The tubing delay of formic acid was determined when its mixing

321 ratios reached 90% of the change before entering the tubing. However, the long-tail
322 memory effect of the tubing mainly focused on the rest 10% of the change (Figure 1),
323 which required a much longer time to stabilize.

324 Impacts of the tubing memory effects will be accumulated due to the continuous
325 change in ambient concentrations of formic acid. To further assess the impacts of tubing
326 memory effects on measurement uncertainties of the two acids, differences between
327 mixing ratios of the species X (namely formic and isocyanic acids) measured with and
328 without long tubes at time t (denoted by $\delta[X]_t$) were calculated using Eq. (1):

$$329 \quad \delta[X]_t = [X_{without}]_t - [X_{with}]_t \quad (1)$$

330 where $[X_{with}]_t$ and $[X_{without}]_t$ refer to mixing ratios of the species X measured at
331 time t with and without long tubes, respectively. In addition, the changes in mixing
332 ratios of the species X measured using long tubes was also calculated using Eq. (2):

$$333 \quad \Delta[X]_t = [X_{with}]_t - \frac{\sum_{t-\Delta t}^t [X_{with}]}{\Delta t} \quad (2)$$

334 where Δt is the change in time relative to time t and was used to characterize the
335 influential time of the memory effect. A strong correlation between $\delta[X]_t$ and $\Delta[X]_t$
336 could be captured at a certain Δt if the tubing memory effect make essential
337 contributions to measurement uncertainties of the species X after traversing long tubes.
338 For the 400 m long tubing, $\delta[X]_t$ and $\Delta[X]_t$ had the strongest correlation ($R^2=0.89$)
339 when Δt was approximately 14 h (Figure S7). As also shown in Figure 2(a), the
340 mixing ratios of formic acid measured with and without the 400 m long tube agreed
341 well when $\Delta[HCOOH]$ approached to zero. The decrease and increase in $\Delta[HCOOH]$
342 will enlarge measurement uncertainties of formic acid using the long tube. In morning
343 periods, ambient mixing ratios of formic acid rapidly increased. As a result, the mixing
344 ratios of formic acid measured through the 400 m long tube were slightly lower than its
345 ambient mixing ratios due to the absorption of formic acid by tubing inner walls. In
346 evening and nighttime periods, an opposite phenomenon was observed due to the
347 desorption of formic acid from tubing inner walls (Figure S4).

348 In addition to the 400 m long tube, impacts of the tubes with lengths of 100, 200,

349 and 300 m on measurements of formic acid were also assessed, as shown in Figures 2(c)
350 and 3(a). The usage of tubes with lengths of 100, 200, and 300 m has negligible impacts
351 on the measurements of formic acid. During the test of the 200 m tubing, meteorological
352 conditions significantly changed with lower temperatures and stronger winds in
353 comparison to the days on which the tests of the other lengths of tubes were performed.
354 As shown in Figure S5, the concentrations of formic acid and isocyanic acid were
355 evidently enhanced and significantly varied during the 400 m tubing test. In contrast,
356 ambient concentrations of formic and isocyanic acid were relatively low and slightly
357 varied, resulting in the exceedingly large or low values of k and R^2 between the
358 concentrations of formic acid measured with and without the 200 m long tubing.
359 However, according to the results of the test, the average concentration difference of
360 formic and isocyanic acid measured with and without the 200 m tubing agreed well
361 within 4%, suggesting that the 200 m long tube has minor effects on the measurements
362 of formic and isocyanic acid.

363 In contrast to formic acid, the usage of long tubes had minor impacts on the
364 measurements of isocyanic acid. The mixing ratios of isocyanic acid measured with and
365 without the 400 m long tube varied consistently ($k=0.86$, $R^2=0.90$) with mean values of
366 0.25 and 0.26 ppbv, respectively (Figure S4). As shown in Figure 2(b), $\Delta[HNCO]$ is
367 evenly distributed on both sides of the 1:1 line. Therefore, the changes in ambient
368 concentrations of isocyanic acid do not have significant impacts on the measurements
369 of isocyanic acid through the long tubes. As also shown in Figure 3(b), $\delta[HNCO]$ and
370 $\Delta[HNCO]$ of isocyanic acid were independent of the changes in isocyanic acid mixing
371 ratios. The R^2 values of linear fittings were less than 0.21 for the isocyanic acid
372 measurements made using different lengths of tubes. This is consistent with the results
373 reported in the literature (*Helmig et al., 2008a; Helmig et al., 2008b; Li et al., 2023*)
374 that inorganic species with low reactivities can be well measured using long PFA Teflon
375 tubes. The test results confirmed that the measurements of formic acid and isocyanic
376 acid through long tubes can be used to characterize their vertical and temporal

377 variability. However, a further correction of the formic acid measurements made
378 through the long tubes must be performed if they were used to accurately calculate the
379 kinetic parameters of chemical reactions regarding the formation and removal of formic
380 acid at different heights.

381 **3.2. Vertical variations and sources of formic acid**

382 Time series of formic acid and ozone mixing ratios at 5 and 320 m are shown in
383 Figure 4. The concentrations of formic acid and ozone exhibited similar diurnal and
384 inter-diurnal variations at different altitudes during the campaign. Hourly mean mixing
385 ratios of ozone exhibited strong temporal variations with an average of 43.5 ± 25.3 ppbv
386 at 5 m and an average of 53.5 ± 25.0 ppbv at 320 m. Hourly mean mixing ratios of formic
387 acid at 5 m ranged between 0.1-6.6 ppbv with an average of 1.3 ± 1.3 ppbv at 5 m, which
388 is comparable to those observed in other megacities, such as Shenzhen (1.2 ppbv) in
389 China (*Zhu et al., 2019*), London (1.3 ppbv) in UK (*Bannan et al., 2017*), and Los
390 Angeles (2.0 ppbv) in USA (*Yuan et al., 2015*). By contrast, hourly mean mixing ratios
391 of formic acid at 320 m had an average of 2.1 ± 1.9 ppbv, approximately 1.6 times higher
392 than that at 5 m. The temporal variability of formic and isocyanic acids were mainly
393 caused by the diurnal and inter-diurnal changes in meteorological conditions (e.g., solar
394 radiation and PBLH).

395 Before July 12th, the daily maximum hourly mixing ratios of ozone at 5 m all
396 exceeded 100 ppbv, indicating the enhanced formation of secondary air pollutants
397 associated with photochemical reactions. The mixing ratios of formic acid measured
398 before July 12th were also prominently larger than those measured after, suggesting
399 important contributions from photochemical formations. The photochemical formation
400 of secondary pollutants was weak from July 13th to 30th due to the cloudy and rainy
401 weather. After August 1st, low mixing ratios of ozone and formic acids were observed
402 along with the occurrence of favorable dilution conditions characterized by high PBLHs.

403 As shown in Figure 5, the mixing ratios of formic acid measured at the five
404 altitudes (namely 5, 47, 102, 200, and 320 m) exhibited similar diurnal patterns. After

405 sunrise (~6:00 LT), formic acid mixing ratios increased rapidly at each altitude before
406 reaching the peak between 14:00-16:00 LT and then continuously declined before
407 sunrise the following day. Similar diurnal variation patterns of formic acid were also
408 observed at other urban sites (*Veres et al., 2011*), rural sites (*Hu et al., 2022*), and remote
409 sites (*Schobesberger et al., 2016*). The diurnal variation patterns of formic acid were
410 highly similar to those of ozone (a typical secondary pollutant) but were different from
411 those of VOCs from primary emissions. Taking toluene as an example, toluene is a
412 typical VOC tracer of anthropogenic emission sources in urban regions, such as
413 industrial processes and vehicular exhausts (*Fang et al., 2016; Skorokhod et al., 2017*),
414 and is also an important precursor of ozone (*Yuan et al., 2012*). The mixing ratios of
415 toluene exhibited opposite diurnal variation patterns to those of ozone and formic acids
416 with the minima occurring at around 14:00 LT. The lower mixing ratios of toluene in
417 daytime than in nighttime were predominantly caused by the enhancement of
418 atmospheric dilution and chemical removal by OH radicals (*De Gouw et al., 2018*). The
419 mixing ratios of formic acid poorly correlated (R^2 ranged between 0.16-0.28) with those
420 of CO (a typical tracer of combustion sources) at the five altitudes but well correlated
421 (R^2 ranged between 0.67-0.75) with those of O_x (O₃+NO₂, a conserved metric of ozone
422 by removing NO titration effect), as shown in Figure 6. These results further confirm
423 that ambient concentrations of formic acid in urban Beijing were dominantly
424 contributed by secondary sources associated with photochemical reactions rather than
425 primary emissions.

426 Another observed evidence for the dominant contribution of formic acid from
427 secondary formations is its positive vertical gradients in nighttime (defined as the
428 period of 22:00-5:00 LT), as shown in Figure 7. Large amounts of formic acid will
429 accumulate near the surface with strong negative vertical gradients if primary emissions
430 dominate its contributions, as manifested by vertical toluene profiles. At nighttime, the
431 mixing ratios of ozone also increased with height due to enhanced removal by NO
432 titration and surface dry deposition. The deposition of formic acid was also enhanced

433 near the surface, driving the formation of positive gradients in vertical formic acid
434 profiles.

435 A notable difference existed between the diurnal variation patterns of ozone and
436 formic acid above the ground. As shown in Figure 5, the mean mixing ratios of ozone
437 at 5 m rapidly increased from 21.5 ppbv to 36.0 ppbv from 6:00 to 10:00 LT, while the
438 mean mixing ratios of ozone at 320 m slightly increased from 16.3 ppbv to 16.9 ppbv
439 during the same period. The enhancement rate is defined as the average change rate of
440 the species concentration between two adjacent hours. As shown in Figure 8, the
441 enhancement rates of ozone mixing ratios between 6:00 and 10:00 LT decreased with
442 the increase in height. This phenomenon indicates relatively weak photochemical ozone
443 formation in urban regions aloft before 10:00 LT due to the lack of reactive ozone
444 precursors (e.g., unsaturated hydrocarbons and NO_x). With the enhancement of the
445 vertical exchange of air masses with the rise of the boundary layer, large amounts of
446 ozone precursors (e.g., the observed peaks of toluene mixing ratios at 320 m at 10:00
447 LT) emitted from surface sources were transported upward and drove the formation of
448 ozone in high altitudes. In contrast to ozone, the mixing ratios of formic acid at the five
449 altitudes all increased rapidly between 6:00 and 10:00 LT. The enhancement rate of
450 formic acid mixing ratios between 6:00 and 10:00 LT kept nearly constant below 320
451 m (Figure 8). This result implies that the oxidation products of VOCs over nighttime or
452 in the daytime before are important precursors of formic acid and can drive the rapid
453 formation of formic acid with further photooxidation. This speculation can be supported
454 by the vertical and diurnal variations of methyl vinyl ketone (MVK), methacrolein
455 (MACR), and formaldehyde, which are reported key precursors of formic acid as shown
456 in Figure 5(d) and 5(e). The diurnal variation patterns of MVK+MACR and
457 formaldehyde at the five latitudes were nearly the same with the enhancements in
458 daytime. In addition, concentrations of MVK+MACR and formaldehyde all increased
459 with height in nighttime and early morning periods, facilitating the photochemical
460 formation of formic acid even in the residual layer.

461 As a reactive hydrocarbon species, the mixing ratios of toluene rapidly decreased
462 with height in daytime (defined as the period of 11:00-16:00 LT, as shown in Figure 7)
463 due to the combined effects of atmospheric dilution and OH-initiated chemical removal.
464 By contrast, the mixing ratios of ozone and formic acid increased with height. The
465 mixing ratios of ozone and formic acid all rapidly increased with height below 102 m,
466 predominantly attributed to the reduced effect of surface dry deposition with the
467 increase in height. The mean mixing ratios of formic acid increased by 18% from 102
468 m to 320 m in daytime, while ozone mixing ratios were well mixed above 102 m. Our
469 results point to the likely importance of photochemistry as a source of formic acid that
470 is enhanced with increasing height within the boundary layer.

471 The precursors and formation mechanisms of atmospheric formic acid have been
472 extensively investigated in previous studies but still remain uncertain. Isoprene has long
473 been recognized as an important precursor of formic acid through reactions with O₃ and
474 OH radicals (*Neeb et al., 1997; Paulot et al., 2009*). Recent studies also found that the
475 degradation of organic aerosols (OA) derived from isoprene is an important source of
476 formic acid (*Cope et al., 2021; Bates et al., 2023*). In addition, the photooxidation of
477 other biogenic and anthropogenic hydrocarbons is also a key source of formic acid
478 (*Paulot et al., 2011; Millet et al., 2015; Link et al., 2021*). Figure 9 illustrates the mean
479 vertical profiles of several key precursors of formic acid in daytime. The concentrations
480 of isoprene and toluene (Figure 7) all decreased rapidly with height. By contrast, MVK
481 and MACR, the primary oxidation products of isoprene (*Grosjean et al., 1993*),
482 exhibited weak vertical gradients. Formaldehyde, a more general photooxidation
483 product of VOCs, exhibited similar vertical distribution patterns to those of ozone.
484 Large amounts of OVOCs were produced and accumulated in higher altitudes through
485 the oxidation of hydrocarbons and the further oxidation of some OVOCs during their
486 upward mixing course. MVK, MACR, and formaldehyde are also key precursors of
487 formic acid. MVK and MACR can react with O₃ to produce formic acid (*Link et al.,*
488 *2020*). Formaldehyde can be converted to methanediol in cloud droplets and then be

489 rapidly oxidized by OH to produce formic acid (*Franco et al., 2021*). In addition, enol
490 (*Lei et al., 2020*) and many other OVOCs (such as glycolaldehyde (*Butkovskaya et al.,*
491 *2006a*) and hydroxyacetone (*Butkovskaya et al., 2006b*) can be further oxidized to
492 produce formic acid. Therefore, high concentrations of OVOCs aloft may be the
493 dominant factor that largely enhances the photochemical formation of formic acid in
494 urban regions.

495 As discussed above, formic acid exhibited strong positive vertical gradients
496 throughout the day, implying that the concentrations of formic acid measured at ground
497 level were not capable of accurately characterizing its abundance and temporal
498 variability in the whole boundary layer. Besides, the formic acid formed in daytime and
499 retained in the nocturnal residual layer also has vital impacts on the budget of formic
500 acid in the boundary layer. Thus, we used the column-integrated concentration (CIC)
501 of formic acid (the sum of the abundance in both the nocturnal residual layer and the
502 boundary layer, see detailed definitions in SI) to further clarify the diurnal variability
503 in the abundance of formic acid in the boundary layer.

504 As shown in Figure 10, the CICs of formic acid had a flatter diurnal pattern in
505 comparison to those at ground level. The CICs of formic acid had approximately stable
506 values overnight and reached a maximum at 16:00 LT. The ratio of the maximum and
507 minimum of CIC for formic acid was only 1.3, while it was 4.2 for the concentrations
508 of formic acid at 5 m. The ground-level measurements were more affected by
509 depositional losses, while such depositional losses in the residual layer were nearly
510 absent. However, the chemical species retained in the residual layer were closely related
511 to their budgets in the daytime boundary layer. If the removal rates of formic acid from
512 ground-level measurements were used to characterize those at high altitudes (e.g., in
513 the residual layer), the removal of formic acid in the entire boundary layer would be
514 overestimated. As the result, numerical models cannot accurately reproduce the
515 abundances and budgets of formic acid without the constraints of vertical observations
516 and the clarification of formic acid formation mechanisms.

517 **3.3. Vertical variations and sources of isocyanic acid**

518 The mixing ratios of isocyanic acid also exhibited strong temporal variations
519 during the campaign with a mean of 0.28 ± 0.16 ppbv at 5 m and a mean of 0.43 ± 0.21
520 ppbv at 320 m, as shown in Figure 11. The mixing ratios of isocyanic acid measured at
521 the ground level in urban Beijing were approximately 10 times higher than those
522 measured in Los Angeles, USA (0.025 ppbv) (Roberts *et al.*, 2014) and Calgary, Canada
523 (0.036 ppbv) (Woodward-Massey *et al.*, 2014) but were lower than those measured in
524 other regions in China. For example, the mean mixing ratio of isocyanic acid was 0.37
525 ppbv at a rural site (Gucheng) in the North China Plain (NCP), and 0.46 ppbv in urban
526 Guangzhou in the Pearl River Delta (PRD) region (Wang *et al.*, 2020). Isocyanic acid
527 will pose a threat to human health when its ambient mixing ratios exceed 1.0 ppbv. In
528 this study, isocyanic acid mixing ratios greater than 1.0 ppbv were not observed at
529 ground level but were observed at 320 m on three days. The maximum hourly mixing
530 ratios of isocyanic acid at 320 m reached 1.63 ppbv at 16:00 LT on July 8th.

531 The mixing ratios of isocyanic acid at the five altitudes exhibited similar diurnal
532 variation patterns. After sunrise, the mixing ratios of isocyanic acid at the five altitudes
533 all simultaneously increased and peaked at about 14:00 LT. Then, isocyanic acid mixing
534 ratios decreased slowly and reached the minimum before sunrise the following day.
535 This diurnal variation pattern of isocyanic acid measured at the ground level in urban
536 Beijing was not consistent with those measured at the Gucheng site in NCP (Wang *et al.*
537 *et al.*, 2020). The isocyanic acid mixing ratios at the Gucheng site exhibited insignificant
538 diurnal variability throughout the day with only a weak morning peak, predominantly
539 attributed to the enhancement of primary emissions. However, the diurnal variation
540 patterns of isocyanic acid measured at the five altitudes were well correlated with the
541 change in solar irradiance and were consistent with those measured at the two sites in
542 PRD. These results imply that ambient concentrations of isocyanic acid in urban Beijing
543 were mainly contributed by secondary sources associated with photochemical reactions.

544 Similar to formic acid, the simultaneous increase of isocyanic acid mixing ratios

545 at the five altitudes with the onset of sunlight also indicates the presence of adequate
546 precursors even in the nocturnal residual layer. In addition, the diurnal variability of
547 isocyanic acid mixing ratios measured below 200 m was much weaker than those
548 measured at 320 m. For example, the ratio of the daily maximum to the daily minimum
549 mixing ratios of isocyanic acid was 1.9 at 320 m, while the ratio was only 1.4 at 5 m.
550 The mean enhancement rate of isocyanic acid mixing ratios at 320 m (0.05 ppbv h^{-1})
551 between 6:00 and 10:00 LT was approximately five times larger than that at 5 m (0.01
552 ppbv h^{-1}). The vertical gradients of isocyanic acid between 102 and 320 m were also
553 larger than those below (Figure 12). The rapid increase in both concentrations and
554 enhancement rates of isocyanic acid with height (Figures 8 and 12) implies the
555 enhanced photochemical formation of isocyanic acid in the middle and upper part of
556 the boundary layer.

557 Secondary formation precursors of atmospheric isocyanic acid were still poorly
558 understood so far. Amides were considered important precursors of isocyanic acid
559 (*Roberts et al., 2014; Rosanka et al., 2020*). As reported in our previous study (*Wang*
560 *et al., 2020*), C_3 amides accounted for the largest fraction of the total concentrations of
561 amides and were dominant contributors to the secondary formation of isocyanic acid.
562 The mixing ratios of C_3 amides in Guangzhou in PRD exhibited strong diurnal
563 variations. Along with the sunrise, the mixing ratios of C_3 amides rapidly decreased and
564 reached the minimum at 13:00 LT. Afterward, the mixing ratios of C_3 amides started to
565 increase and accumulated at night. As shown in Figure S6, the influence of long tubing
566 on the measurement of amides was limited, so we also measured the amides during the
567 field campaign. However, the mixing ratios of C_3 amides in Beijing and Gucheng in
568 NCP exhibited insignificant diurnal variability, consistent with those of isocyanic acid.
569 The mean mixing ratios of C_3 amides at 5 m in urban Beijing is only 0.03 ppbv during
570 the campaign, which is one order of magnitude lower than those in Guangzhou (0.35
571 ppbv) and Gucheng (0.18 ppbv). The mixing ratios of C_3 amides measured at the five
572 altitudes in urban Beijing were also approximately one order of magnitude lower than

573 those of isocyanic acid (Figure 12). Besides, the mixing ratios of C₃ amides decreased
574 with height in both nighttime and daytime, indicating predominant contributions from
575 primary emissions. This is consistent with the fact that primary emissions of chemical
576 composition from industry-related sources have been largely reduced with the outward
577 migration of industry in urban Beijing. By contrast, the mixing ratios of isocyanic acid
578 increased with height in both day and night with an average of 0.32 ppbv at 5 m and
579 0.60 ppbv at 320 m. These results suggest that C₃ amides were far more enough to
580 account for the secondary formation of isocyanic acid in urban Beijing.

581 Figure 13(a) gives the composition and average concentrations of C₁-C₁₀ amides
582 measured at the five altitudes during the campaign. C₂ amides accounted for the largest
583 fraction of the total mixing ratios of amides. The total mixing ratios of amides exhibited
584 decreasing tendencies with the increase in height, suggesting predominant contributions
585 from direct emissions of surface sources. As for formamide, its mixing ratios exhibited
586 an increasing tendency from 0.024 ppbv at 5 m to 0.030 ppbv at 320 m. The positive
587 vertical gradients of formamide suggest its enhanced formation with height, probably
588 due to the enhancements of formic acid. However, the average concentration ratios of
589 formamide to formic acid slightly varied between 0.01 and 0.02 among the five heights.
590 The average concentration ratios of formamide to isocyanic acid decreased from 0.09
591 at 5 m to 0.07 at 320 m. These results imply that the formation of isocyanic acid through
592 the pathway of HCOOH-CH₃NO-HNCO may be enhanced with the increase in height
593 but could only contribute a tiny fraction of the observed isocyanic acid, as shown in
594 Figure 13(b). Assuming the full conversion of C₁-C₁₀ amides to isocyanic acid, the
595 average concentration ratios of amides (sum of C₁-C₁₀) to isocyanic acid below 320 m
596 only ranged between 0.32 and 0.56 and decreased with height. Therefore, in addition to
597 amides, there must be other important precursors and formation pathways of isocyanic
598 acid, particularly in high altitudes. The simultaneous increase of isocyanic acid
599 concentrations at the five heights upon sunrise (Figure 11) implies the presence of
600 adequate precursors in the nocturnal residual layer. The oxidation products of VOCs

601 driven by ozone and NO_3 radicals in nighttime may be an important class of precursors.
602 In addition, the largest enhancement rates and highest concentrations of isocyanic acid
603 at 320 m in daytime also suggest that high concentrations of OVOCs and low- NO_x
604 conditions may enhance the secondary formation of isocyanic acid.

605 The positive vertical gradients of isocyanic acid imply that the secondary
606 formation of isocyanic acid aloft could serve as an important source of surface isocyanic
607 acid in daytime driven by turbulence mixing. The CICs of isocyanic acid were
608 calculated to further clarify its abundance and temporal variability in the whole
609 boundary layer. Distinct diurnal patterns were observed between the ground-level
610 concentrations and CICs of isocyanic acid. Analogous to formic acid, the CICs of
611 isocyanic acid varied insignificantly over nighttime and enhanced in daytime, reaching
612 the maximum at approximately 14:00 LT. The formation of some chemicals can be
613 largely enhanced at higher altitudes and so using ground-level measurements to
614 constrain numerical models may be not adequate.

615 **4. Conclusion**

616 In this study, vertical and diurnal variations of formic and isocyanic acids in
617 urban Beijing were investigated using tower-based online gradient measurements. The
618 measurements of isocyanic acid can be well measured through long PFA Teflon tubes.
619 The measurements of formic acid made through long tubes were slightly influenced by
620 the memory effect of tubing walls, and the vertical increasing gradients of formic acid
621 may be slightly enhanced if the tubing effects were considered. The concentrations of
622 formic and isocyanic acids all increased with height in both nighttime and daytime. The
623 diurnal and vertical distribution patterns of formic and isocyanic acids all suggest that
624 their abundances in the boundary layer were dominantly contributed by secondary
625 formation associated with photochemical reactions. The photochemical formations of
626 formic and isocyanic acids were also substantially enhanced with the increase in height.
627 The formation pathway of isocyanic acid through $\text{HCOOH-CH}_3\text{NO-HNCO}$ only

628 accounted for a tiny fraction of its ambient abundance. The formic and isocyanic acids
629 photochemically formed in the middle and upper parts of the boundary layer were
630 important sources for those at ground level in urban region. The differences of the
631 diurnal patterns between CICs and ground-level concentrations of formic and isocyanic
632 acids further highlight the importance of vertical observations in elucidating their
633 budgets and sources in the whole boundary layer.

634 Characterization of the vertical variations in formic and isocyanic acids could
635 provide valuable information for elucidating their budgets and sources in the boundary
636 layer. However, there are still many important but unresolved questions associated with
637 the vertical distributions of formic and isocyanic acids. For example, the key precursors
638 that drive the rapid formation of formic and isocyanic acids in the residual layer are still
639 unknown. Are there any changes in the key precursors and formation pathways of
640 formic and isocyanic acids with the increase of height in urban region? To answer these
641 questions, the combination of vertical gradient measurements of more chemical species
642 and numerical simulations is needed in future studies.

643 **Supporting Information:** Additional experimental details, materials, and methods,
644 including schematic illustration of tubing test, determination of the long tubes'
645 cumulative influence, and calculation of CICs.

646 **Data availability**

647 Data related to this article are available online at
648 <https://doi.org/10.7910/DVN/ANH0WE>.

649 **Author contributions**

650 QY, XBL, BY, and YH designed the research. QY, XBL, BY, XZ, YH, LY, XH,
651 JQ and MS contributed to the data collection and data analysis. QY and XBL wrote the
652 paper with contributions from all coauthors. All the coauthors discussed the results and
653 reviewed the paper.

654 **Competing interests**

655 The authors declare that they have no conflict of interest.

656 **Acknowledgment**

657 This work was financially supported by the National Key R&D Plan of China
658 (grant No. 2023YFC3706103, 2023YFC3706201, 2022YFC3700604) and the National
659 Natural Science Foundation of China (grant No. 42121004, 42275103, 42205094,
660 42230701, 42305095). This work was also supported by the Special Fund Project for
661 Science and Technology Innovation Strategy of Guangdong Province (Grant No.
662 2019B121205004). The authors would like to thank the personnel who participated in
663 data collection, instrument maintenance, and logistic support during the field campaign.

664 **Reference**

- 665 Acton, W. J. F., Huang, Z., Davison, B., Drysdale, W. S., Fu, P., Holloway, M., Langford,
666 B., Lee, J., Liu, Y., Metzger, S., Mullinger, N., Nemitz, E., Reeves, C. E., Squires, F.
667 A., Vaughan, A. R., Wang, X., Wang, Z., Wild, O., Zhang, Q., Zhang, Y., and Hewitt,
668 C. N.: Surface–atmosphere fluxes of volatile organic compounds in Beijing,
669 Atmospheric Chemistry and Physics, 20, 15101-15125, 10.5194/acp-20-15101-2020,
670 2020.
- 671 Alwe, H. D., Millet, D. B., Chen, X., Raff, J. D., Payne, Z. C., and Fledderman, K.:
672 Oxidation of Volatile Organic Compounds as the Major Source of Formic Acid in a
673 Mixed Forest Canopy, Geophysical Research Letters, 46, 2940-2948,
674 <https://doi.org/10.1029/2018GL081526>, 2019.
- 675 Andreae, M. O., Talbot, R. W., Andreae, T. W., and Harriss, R. C.: Formic and acetic
676 acid over the central Amazon region, Brazil: 1. Dry season, Journal of Geophysical
677 Research: Atmospheres, 93, 1616-1624, <https://doi.org/10.1029/JD093iD02p01616>,
678 1988.
- 679 Bannan, T. J., Bacak, A., Muller, J. B. A., Booth, A. M., Jones, B., Le Breton, M.,
680 Leather, K. E., Ghalaieny, M., Xiao, P., Shallcross, D. E., and Percival, C. J.:
681 Importance of direct anthropogenic emissions of formic acid measured by a chemical
682 ionisation mass spectrometer (CIMS) during the Winter ClearfLo Campaign in
683 London, January 2012, Atmospheric Environment, 83, 301-310,
684 10.1016/j.atmosenv.2013.10.029, 2014.
- 685 Bannan, T. J., Murray Booth, A., Le Breton, M., Bacak, A., Muller, J. B. A., Leather, K.
686 E., Khan, M. A. H., Lee, J. D., Dunmore, R. E., Hopkins, J. R., Fleming, Z. L., Sheps,
687 L., Taatjes, C. A., Shallcross, D. E., and Percival, C. J.: Seasonality of Formic Acid

688 (HCOOH) in London during the ClearfLo Campaign, *Journal of Geophysical*
689 *Research: Atmospheres*, 122, 10.1002/2017jd027064, 2017.

690 Barnes, I., Solignac, G., Mellouki, A., and Becker, K. H.: Aspects of the atmospheric
691 chemistry of amides, *ChemPhyChem*, 11, 3844-3857, 10.1002/cphc.201000374,
692 2010.

693 Bates, K. H., Jacob, D. J., Cope, J. D., Chen, X., Millet, D. B., and Nguyen, T. B.:
694 Emerging investigator series: aqueous oxidation of isoprene-derived organic aerosol
695 species as a source of atmospheric formic and acetic acids, *Environmental Science:*
696 *Atmospheres*, 10.1039/d3ea00076a, 2023.

697 Benish, S. E., He, H., Ren, X., Roberts, S. J., Salawitch, R. J., Li, Z., Wang, F., Wang,
698 Y., Zhang, F., Shao, M., Lu, S., and Dickerson, R. R.: Measurement report: Aircraft
699 observations of ozone, nitrogen oxides, and volatile organic compounds over Hebei
700 Province, China, *Atmospheric Chemistry and Physics*, 20, 14523-14545,
701 10.5194/acp-20-14523-2020, 2020.

702 Borduas, N., Murphy, J. G., Wang, C., Silva, G. d., Abbatt, J. P. D. J. E. S., and Letters,
703 T.: Gas Phase Oxidation of Nicotine by OH Radicals: Kinetics, Mechanisms, and
704 Formation of HNCO, 3, 327-331, 2016.

705 Butkovskaya, N. I., Pouvesle, N., Kukui, A., and Le Bras, G.: Mechanism of the OH-
706 Initiated Oxidation of Glycolaldehyde over the Temperature Range 233–296 K, *The*
707 *Journal of Physical Chemistry A*, 110, 13492-13499, 10.1021/jp064993k, 2006a.

708 Butkovskaya, N. I., Pouvesle, N., Kukui, A., Mu, Y., and Le Bras, G.: Mechanism of
709 the OH-Initiated Oxidation of Hydroxyacetone over the Temperature Range 236–298
710 K, *The Journal of Physical Chemistry A*, 110, 6833-6843, 10.1021/jp056345r, 2006b.

711 Chandra, B. P. and Sinha, V.: Contribution of post-harvest agricultural paddy residue
712 fires in the N.W. Indo-Gangetic Plain to ambient carcinogenic benzenoids, toxic
713 isocyanic acid and carbon monoxide, *Environment International*, 88, 187-197,
714 10.1016/j.envint.2015.12.025, 2016.

715 Chebbi, A. and Carlier, P.: Carboxylic acids in the troposphere, occurrence, sources,
716 and sinks: A review, *Atmospheric Environment*, 30, 4233-4249,
717 [https://doi.org/10.1016/1352-2310\(96\)00102-1](https://doi.org/10.1016/1352-2310(96)00102-1), 1996.

718 Cope, J. D., Abellar, K. A., Bates, K. H., Fu, X., and Nguyen, T. B.: Aqueous
719 Photochemistry of 2-Methyltetrol and Erythritol as Sources of Formic Acid and
720 Acetic Acid in the Atmosphere, *ACS Earth and Space Chemistry*, 5, 1265-1277,
721 10.1021/acsearthspacechem.1c00107, 2021.

722 De Gouw, J. A., Gilman, J. B., Kim, S. W., Alvarez, S. L., Dusanter, S., Graus, M.,
723 Griffith, S. M., Isaacman - VanWertz, G., Kuster, W. C., Lefer, B. L., Lerner, B. M.,
724 McDonald, B. C., Rappenglück, B., Roberts, J. M., Stevens, P. S., Stutz, J., Thalman,
725 R., Veres, P. R., Volkamer, R., Warneke, C., Washenfelder, R. A., and Young, C. J.:
726 Chemistry of Volatile Organic Compounds in the Los Angeles Basin: Formation of
727 Oxygenated Compounds and Determination of Emission Ratios, *Journal of*
728 *Geophysical Research: Atmospheres*, 123, 2298-2319, 10.1002/2017jd027976, 2018.

729 Deming, B. L., Pagonis, D., Liu, X., Day, D. A., Talukdar, R., Krechmer, J. E., de Gouw,

730 J. A., Jimenez, J. L., and Ziemann, P. J.: Measurements of delays of gas-phase
731 compounds in a wide variety of tubing materials due to gas-wall interactions,
732 Atmospheric Measurement Techniques, 12, 3453-3461, 10.5194/amt-12-3453-2019,
733 2019.

734 Enders, G., Dlugi, R., Steinbrecher, R., Clement, B., Daiber, R., Eijk, J. v., Gäb, S.,
735 Haziza, M., Helas, G., Herrmann, U., Kessel, M., Kesselmeier, J., Kotzias, D.,
736 Kourtidis, K., Kurth, H. H., McMillen, R. T., Roider, G., Schürmann, W., Teichmann,
737 U., and Torres, L.: Biosphere/Atmosphere interactions: Integrated research in a
738 European coniferous forest ecosystem, Atmospheric Environment, 26, 171-189,
739 [https://doi.org/10.1016/0960-1686\(92\)90269-Q](https://doi.org/10.1016/0960-1686(92)90269-Q), 1992.

740 Fang, X., Shao, M., Stohl, A., Zhang, Q., Zheng, J., Guo, H., Wang, C., Wang, M., Ou,
741 J., Thompson, R. L., and Prinn, R. G.: Top-down estimates of benzene and toluene
742 emissions in the Pearl River Delta and Hong Kong, China, Atmospheric Chemistry
743 and Physics, 16, 3369-3382, 10.5194/acp-16-3369-2016, 2016.

744 Franco, B., Blumenstock, T., Cho, C., Clarisse, L., Clerbaux, C., Coheur, P. F., De
745 Mazière, M., De Smedt, I., Dorn, H. P., Emmerichs, T., Fuchs, H., Gkatzelis, G.,
746 Griffith, D. W. T., Gromov, S., Hannigan, J. W., Hase, F., Hohaus, T., Jones, N.,
747 Kerkweg, A., Kiendler-Scharr, A., Lutsch, E., Mahieu, E., Novelli, A., Ortega, I.,
748 Paton-Walsh, C., Pommier, M., Pozzer, A., Reimer, D., Rosanka, S., Sander, R.,
749 Schneider, M., Strong, K., Tillmann, R., Van Roozendaal, M., Vereecken, L.,
750 Vigouroux, C., Wahner, A., and Taraborrelli, D.: Ubiquitous atmospheric production
751 of organic acids mediated by cloud droplets, Nature, 593, 233-237, 10.1038/s41586-
752 021-03462-x, 2021.

753 Fulgham, S. R., Brophy, P., Link, M., Ortega, J., Pollack, I., and Farmer, D. K.: Seasonal
754 Flux Measurements over a Colorado Pine Forest Demonstrate a Persistent Source of
755 Organic Acids, ACS Earth and Space Chemistry, 3, 2017-2032,
756 10.1021/acsearthspacechem.9b00182, 2019.

757 Galloway, J. N., Likens, G. E., Keene, W. C., and Miller, J. M.: The composition of
758 precipitation in remote areas of the world, Journal of Geophysical Research: Oceans,
759 87, 8771-8786, <https://doi.org/10.1029/JC087iC11p08771>, 1982.

760 Goode, J. G., Yokelson, R. J., Ward, D. E., Susott, R. A., Babbitt, R. E., Davies, M. A.,
761 and Hao, W. M.: Measurements of excess O₃, CO₂, CO, CH₄, C₂H₄, C₂H₂, HCN, NO,
762 NH₃, HCOOH, CH₃COOH, HCHO, and CH₃OH in 1997 Alaskan biomass burning
763 plumes by airborne Fourier transform infrared spectroscopy (AFTIR), Journal of
764 Geophysical Research: Atmospheres, 105, 22147-22166, 10.1029/2000jd900287,
765 2000.

766 Grosjean, D., Williams, E. L., II, and Grosjean, E.: Atmospheric chemistry of isoprene
767 and of its carbonyl products, Environmental Science & Technology, 27, 830-840,
768 10.1021/es00042a004, 1993.

769 Helmig, D., Johnson, B., Oltmans, S., Neff, W., Eisele, F., and Davis, D.: Elevated
770 ozone in the boundary layer at South Pole, Atmospheric Environment, 42, 2788-2803,
771 10.1016/j.atmosenv.2006.12.032, 2008a.

772 Helmig, D., Johnson, B., Warshawsky, M., Morse, T., Neff, W., Eisele, F., and Davis,
773 D.: Nitric oxide in the boundary-layer at South Pole during the Antarctic
774 Tropospheric Chemistry Investigation (ANTCI), *Atmospheric Environment*, 42,
775 2817-2830, 10.1016/j.atmosenv.2007.03.061, 2008b.

776 Hems, R. F., Wang, C., Collins, D. B., Zhou, S., Borduas-Dedekind, N., Siegel, J. A.,
777 and Abbatt, J. P. D.: Sources of isocyanic acid (HNCO) indoors: a focus on cigarette
778 smoke, *Environmental Science: Processes & Impacts*, 21, 1334-1341,
779 10.1039/c9em00107g, 2019.

780 Hu, L., Millet, D. B., Kim, S. Y., Wells, K. C., Griffis, T. J., Fischer, E. V., Helmig, D.,
781 Hueber, J., and Curtis, A. J.: North American acetone sources determined from tall
782 tower measurements and inverse modeling, *Atmospheric Chemistry and Physics*, 13,
783 3379-3392, 10.5194/acp-13-3379-2013, 2013.

784 Hu, X., Yang, G., Liu, Y., Lu, Y., Wang, Y., Chen, H., Chen, J., and Wang, L.:
785 Atmospheric gaseous organic acids in winter in a rural site of the North China Plain,
786 *Journal of Environmental Sciences*, 113, 190-203, 10.1016/j.jes.2021.05.035, 2022.

787 Jacob, D. J.: Chemistry of OH in remote clouds and its role in the production of formic
788 acid and peroxymonosulfate, *Journal of Geophysical Research: Atmospheres*, 91,
789 9807-9826, <https://doi.org/10.1029/JD091iD09p09807>, 1986.

790 Jaisson, S., Pietrement, C., and Gillery, P.: Carbamylation-derived products: bioactive
791 compounds and potential biomarkers in chronic renal failure and atherosclerosis,
792 *Clinical chemistry*, 57, 1499-1505, 10.1373/clinchem.2011.163188, 2011.

793 Jathar, S. H., Heppding, C., Link, M. F., Farmer, D. K., Akherati, A., Kleeman, M. J.,
794 de Gouw, J. A., Veres, P. R., and Roberts, J. M.: Investigating diesel engines as an
795 atmospheric source of isocyanic acid in urban areas, *Atmospheric Chemistry and
796 Physics*, 17, 8959-8970, 10.5194/acp-17-8959-2017, 2017.

797 Ji, Y., Huey, L. G., Tanner, D. J., Lee, Y. R., Veres, P. R., Neuman, J. A., Wang, Y., and
798 Wang, X.: A vacuum ultraviolet ion source (VUV-IS) for iodide-chemical ionization
799 mass spectrometry: a substitute for radioactive ion sources, *Atmospheric
800 Measurement Techniques*, 13, 3683-3696, 10.5194/amt-13-3683-2020, 2020.

801 Karion, A., Sweeney, C., Tans, P., and Newberger, T.: AirCore: An Innovative
802 Atmospheric Sampling System, *Journal of Atmospheric and Oceanic Technology*, 27,
803 1839-1853, 10.1175/2010jtecha1448.1, 2010.

804 Kawamura, K. and Kaplan, I. R.: Organic compounds in the rainwater of Los Angeles,
805 *Environmental Science & Technology*, 17, 497-501, 10.1021/es00114a011, 1983.

806 Kawamura, K., Steinberg, S., and Kaplan, I. R.: Homologous series of C₁-C₁₀
807 monocarboxylic acids and C₁-C₆ carbonyls in Los Angeles air and motor vehicle
808 exhausts, *Atmospheric Environment*, 34, 4175-4191, [https://doi.org/10.1016/S1352-
809 2310\(00\)00212-0](https://doi.org/10.1016/S1352-2310(00)00212-0), 2000.

810 Keene, W. C. and Galloway, J. N.: Organic acidity in precipitation of North America,
811 *Atmospheric Environment*, 18, 2491-2497, [https://doi.org/10.1016/0004-
812 6981\(84\)90020-9](https://doi.org/10.1016/0004-6981(84)90020-9), 1984.

813 Kesselmeier, J., Bode, K., Gerlach, C., and Jork, E. M.: Exchange of atmospheric

814 formic and acetic acids with trees and crop plants under controlled chamber and
815 purified air conditions, *Atmospheric Environment*, 32, 1765-1775,
816 [https://doi.org/10.1016/S1352-2310\(97\)00465-2](https://doi.org/10.1016/S1352-2310(97)00465-2), 1998.

817 Khare, P., Kumar, N., Kumari, K. M., and Srivastava, S. S.: Atmospheric formic and
818 acetic acids: An overview, *Reviews of Geophysics*, 37, 227-248,
819 <https://doi.org/10.1029/1998RG900005>, 1999.

820 Koeth, R. A., Kalantar-Zadeh, K., Wang, Z., Fu, X., Tang, W. H., and Hazen, S. L.:
821 Protein carbamylation predicts mortality in ESRD, *Journal of the American Society*
822 *of Nephrology*, 24, 853-861, 10.1681/ASN.2012030254, 2013.

823 Krechmer, J. E., Day, D. A., Ziemann, P. J., and Jimenez, J. L.: Direct Measurements
824 of Gas/Particle Partitioning and Mass Accommodation Coefficients in
825 Environmental Chambers, *Environmental science & technology*, 51, 11867-11875,
826 10.1021/acs.est.7b02144, 2017.

827 Le Breton, M., Bacak, A., Muller, J. B. A., Xiao, P., Shallcross, B. M. A., Batt, R.,
828 Cooke, M. C., Shallcross, D. E., Bauguitte, S. J. B., and Percival, C. J.: Simultaneous
829 airborne nitric acid and formic acid measurements using a chemical ionization mass
830 spectrometer around the UK: Analysis of primary and secondary production
831 pathways, *Atmospheric Environment*, 83, 166-175, 10.1016/j.atmosenv.2013.10.008,
832 2014.

833 Lei, X., Wang, W., Gao, J., Wang, S., and Wang, W.: Atmospheric Chemistry of Enols:
834 The Formation Mechanisms of Formic and Peroxyformic Acids in Ozonolysis of
835 Vinyl Alcohol, *The Journal of Physical Chemistry A*, 124, 4271-4279,
836 10.1021/acs.jpca.0c01480, 2020.

837 Li, T., Wang, Z., Yuan, B., Ye, C., Lin, Y., Wang, S., Sha, Q. e., Yuan, Z., Zheng, J., and
838 Shao, M.: Emissions of carboxylic acids, hydrogen cyanide (HCN) and isocyanic
839 acid (HNCO) from vehicle exhaust, *Atmospheric Environment*, 247,
840 10.1016/j.atmosenv.2021.118218, 2021.

841 Li, X.-B., Yuan, B., Wang, S., Wang, C., Lan, J., Liu, Z., Song, Y., He, X., Huangfu, Y.,
842 Pei, C., Cheng, P., Yang, S., Qi, J., Wu, C., Huang, S., You, Y., Chang, M., Zheng, H.,
843 Yang, W., Wang, X., and Shao, M.: Variations and sources of volatile organic
844 compounds (VOCs) in urban region: insights from measurements on a tall tower,
845 *Atmospheric Chemistry and Physics*, 22, 10567-10587, 10.5194/acp-22-10567-2022,
846 2022.

847 Li, X., Zhang, C., Liu, A., Yuan, B., Yang, H., Liu, C., Wang, S., Huangfu, Y., Qi, J.,
848 Liu, Z., He, X., Song, X., Chen, Y., Peng, Y., Zhang, X., Zheng, E., Yang, L., Yang,
849 Q., Qin, G., Zhou, J., and Shao, M.: Assessment of Long Tubing in Measuring
850 Atmospheric Trace Gases: Applications on Tall Towers, *Environmental Science:*
851 *Atmospheres*, 506-520, 10.1039/d2ea00110a, 2023.

852 Liggio, J., Moussa, S. G., Wentzell, J., Darlington, A., Liu, P., Leithead, A., Hayden, K.,
853 O'Brien, J., Mittermeier, R. L., Staebler, R., Wolde, M., and Li, S.-M.: Understanding
854 the primary emissions and secondary formation of gaseous organic acids in the oil
855 sands region of Alberta, Canada, *Atmospheric Chemistry and Physics*, 17, 8411-8427,

856 10.5194/acp-17-8411-2017, 2017.

857 Link, M. F., Brophy, P., Fulgham, S. R., Murschell, T., and Farmer, D. K.: Isoprene
858 versus Monoterpenes as Gas-Phase Organic Acid Precursors in the Atmosphere, ACS
859 Earth and Space Chemistry, 5, 1600-1612, 10.1021/acsearthspacechem.1c00093,
860 2021.

861 Link, M. F., Nguyen, T. B., Bates, K., Müller, J.-F., and Farmer, D. K.: Can Isoprene
862 Oxidation Explain High Concentrations of Atmospheric Formic and Acetic Acid over
863 Forests?, ACS Earth and Space Chemistry, 4, 730-740,
864 10.1021/acsearthspacechem.0c00010, 2020.

865 Liu, X., Deming, B., Pagonis, D., Day, D. A., Palm, B. B., Talukdar, R., Roberts, J. M.,
866 Veres, P. R., Krechmer, J. E., Thornton, J. A., de Gouw, J. A., Ziemann, P. J., and
867 Jimenez, J. L.: Effects of gas-wall interactions on measurements of semivolatile
868 compounds and small polar molecules, Atmospheric Measurement Techniques, 12,
869 3137-3149, 10.5194/amt-12-3137-2019, 2019.

870 Lopez-Hilfiker, F. D., Mohr, C., Ehn, M., Rubach, F., Kleist, E., Wildt, J., Mentel, T. F.,
871 Lutz, A., Hallquist, M., Worsnop, D., and Thornton, J. A.: A novel method for online
872 analysis of gas and particle composition: description and evaluation of a Filter Inlet
873 for Gases and AEROSols (FIGAERO), Atmospheric Measurement Techniques, 7,
874 983-1001, 10.5194/amt-7-983-2014, 2014.

875 Mattila, J. M., Brophy, P., Kirkland, J., Hall, S., Ullmann, K., Fischer, E. V., Brown, S.,
876 McDuffie, E., Tevlin, A., and Farmer, D. K.: Tropospheric sources and sinks of gas-
877 phase acids in the Colorado Front Range, Atmospheric Chemistry and Physics, 18,
878 12315-12327, 10.5194/acp-18-12315-2018, 2018.

879 Meng, F., Qin, M., Tang, K., Duan, J., Fang, W., Liang, S., Ye, K., Xie, P., Sun, Y., Xie,
880 C., Ye, C., Fu, P., Liu, J., and Liu, W.: High-resolution vertical distribution and
881 sources of HONO and NO₂ in the nocturnal boundary layer in urban Beijing, China,
882 Atmospheric Chemistry and Physics, 20, 5071-5092, 10.5194/acp-20-5071-2020,
883 2020.

884 Millet, D. B., Baasandorj, M., Farmer, D. K., Thornton, J. A., Baumann, K., Brophy, P.,
885 Chaliyakunnel, S., de Gouw, J. A., Graus, M., Hu, L., Koss, A., Lee, B. H., Lopez-
886 Hilfiker, F. D., Neuman, J. A., Paulot, F., Peischl, J., Pollack, I. B., Ryerson, T. B.,
887 Warneke, C., Williams, B. J., and Xu, J.: A large and ubiquitous source of
888 atmospheric formic acid, Atmospheric Chemistry and Physics, 15, 6283-6304,
889 10.5194/acp-15-6283-2015, 2015.

890 Mungall, E. L., Abbatt, J. P. D., Wentzell, J. J. B., Wentworth, G. R., Murphy, J. G.,
891 Kunkel, D., Gute, E., Tarasick, D. W., Sharma, S., Cox, C. J., Uttal, T., and Liggio,
892 J.: High gas-phase mixing ratios of formic and acetic acid in the High Arctic,
893 Atmospheric Chemistry and Physics, 18, 10237-10254, 10.5194/acp-18-10237-2018,
894 2018.

895 Mydel, P., Wang, Z., Brisslert, M., Hellvard, A., Dahlberg, L. E., Hazen, S. L., and
896 Bokarewa, M. I. J. T. J. o. I.: Carbamylation-Dependent Activation of T Cells: A
897 Novel Mechanism in the Pathogenesis of Autoimmune Arthritis, The Journal of

898 Immunology, 184, 6882 - 6890, 2010.

899 Neeb, P., Sauer, F., Horie, O., and Moortgat, G. K.: Formation of hydroxymethyl
900 hydroperoxide and formic acid in alkene ozonolysis in the presence of water vapour,
901 Atmospheric Environment, 31, 1417-1423, [https://doi.org/10.1016/S1352-
902 2310\(96\)00322-6](https://doi.org/10.1016/S1352-2310(96)00322-6), 1997.

903 Pagonis, D., Krechmer, J. E., de Gouw, J., Jimenez, J. L., and Ziemann, P. J.: Effects of
904 gas-wall partitioning in Teflon tubing and instrumentation on time-resolved
905 measurements of gas-phase organic compounds, Atmospheric Measurement
906 Techniques, 10, 4687-4696, 10.5194/amt-10-4687-2017, 2017.

907 Palm, B. B., Liu, X., Jimenez, J. L., and Thornton, J. A.: Performance of a new coaxial
908 ion-molecule reaction region for low-pressure chemical ionization mass
909 spectrometry with reduced instrument wall interactions, Atmospheric Measurement
910 Techniques, 12, 5829-5844, 10.5194/amt-12-5829-2019, 2019.

911 Paulot, F., Crouse, J. D., Kjaergaard, H. G., Kroll, J. H., Seinfeld, J. H., and Wennberg,
912 P. O.: Isoprene photooxidation: new insights into the production of acids and organic
913 nitrates, Atmospheric Chemistry and Physics, 9, 1479-1501, 10.5194/acp-9-1479-
914 2009, 2009.

915 Paulot, F., Wunch, D., Crouse, J. D., Toon, G. C., Millet, D. B., DeCarlo, P. F.,
916 Vigouroux, C., Deutscher, N. M., Gonzalez Abad, G., Notholt, J., Warneke, T.,
917 Hannigan, J. W., Warneke, C., de Gouw, J. A., Dunlea, E. J., De Maziere, M., Griffith,
918 D. W. T., Bernath, P., Jimenez, J. L., and Wennberg, P. O.: Importance of secondary
919 sources in the atmospheric budgets of formic and acetic acids, Atmospheric
920 Chemistry and Physics, 11, 1989-2013, 10.5194/acp-11-1989-2011, 2011.

921 Roberts, J. M. and Liu, Y.: Solubility and solution-phase chemistry of isocyanic acid,
922 methyl isocyanate, and cyanogen halides, Atmospheric Chemistry and Physics, 19,
923 4419-4437, 10.5194/acp-19-4419-2019, 2019.

924 Roberts, J. M., Veres, P. R., Cochran, A. K., Warneke, C., Burling, I. R., Yokelson, R.
925 J., Lerner, B., Gilman, J. B., Kuster, W. C., Fall, R., and de Gouw, J.: Isocyanic acid
926 in the atmosphere and its possible link to smoke-related health effects, Proceedings
927 of the National Academy of Sciences, 108, 8966-8971, 10.1073/pnas.1103352108,
928 2011.

929 Roberts, J. M., Veres, P. R., VandenBoer, T. C., Warneke, C., Graus, M., Williams, E.
930 J., Lefer, B., Brock, C. A., Bahreini, R., Öztürk, F., Middlebrook, A. M., Wagner, N.
931 L., Dubé, W. P., and de Gouw, J. A.: New insights into atmospheric sources and sinks
932 of isocyanic acid, HNCO, from recent urban and regional observations, Journal of
933 Geophysical Research: Atmospheres, 119, 1060-1072, 10.1002/2013jd019931, 2014.

934 Rosanka, S., Vu, G. H. T., Nguyen, H. M. T., Pham, T. V., Javed, U., Taraborrelli, D.,
935 and Vereecken, L.: Atmospheric chemical loss processes of isocyanic acid (HNCO):
936 a combined theoretical kinetic and global modelling study, Atmospheric Chemistry
937 and Physics, 20, 6671-6686, 10.5194/acp-20-6671-2020, 2020.

938 Schnitzhofer, R., Wisthaler, A., and Hansel, A.: Real-time profiling of organic trace
939 gases in the planetary boundary layer by PTR-MS using a tethered balloon,

940 Atmospheric Measurement Techniques, 2, 773-777, 10.5194/amt-2-773-2009, 2009.
941 Schobesberger, S., Lopez - Hilfiker, F. D., Taipale, D., Millet, D. B., D'Ambro, E. L.,
942 Rantala, P., Mammarella, I., Zhou, P., Wolfe, G. M., Lee, B. H., Boy, M., and
943 Thornton, J. A.: High upward fluxes of formic acid from a boreal forest canopy,
944 Geophysical Research Letters, 43, 9342-9351, 10.1002/2016gl069599, 2016.
945 Skorokhod, A. I., Berezina, E. V., Moiseenko, K. B., Elansky, N. F., and Belikov, I. B.:
946 Benzene and toluene in the surface air of northern Eurasia from TROICA-12
947 campaign along the Trans-Siberian Railway, Atmospheric Chemistry and Physics, 17,
948 5501-5514, 10.5194/acp-17-5501-2017, 2017.
949 Stavrou, T., Müller, J. F., Peeters, J., Razavi, A., Clarisse, L., Clerbaux, C., Coheur,
950 P. F., Hurtmans, D., De Mazière, M., Vigouroux, C., Deutscher, N. M., Griffith, D.
951 W. T., Jones, N., and Paton-Walsh, C.: Satellite evidence for a large source of formic
952 acid from boreal and tropical forests, Nature Geoscience, 5, 26-30,
953 10.1038/ngeo1354, 2011.
954 Tan, Q., Ge, B., Xu, X., Gan, L., Yang, W., Chen, X., Pan, X., Wang, W., Li, J., and
955 Wang, Z.: Increasing impacts of the relative contributions of regional transport on air
956 pollution in Beijing: Observational evidence, Environmental Pollution, 292, 118407,
957 10.1016/j.envpol.2021.118407, 2022.
958 Verbrugge, F. H., Tang, W. H., and Hazen, S. L.: Protein carbamylation and
959 cardiovascular disease, Kidney International, 88, 474-478, 10.1038/ki.2015.166,
960 2015.
961 Veres, P. R., Roberts, J. M., Cochran, A. K., Gilman, J. B., Kuster, W. C., Holloway, J.
962 S., Graus, M., Flynn, J., Lefer, B., Warneke, C., and de Gouw, J.: Evidence of rapid
963 production of organic acids in an urban air mass, Geophysical Research Letters, 38,
964 L17807, 10.1029/2011gl048420, 2011.
965 Wang, Z., Nicholls, S. J., Rodriguez, E. R., Kummu, O., Horkko, S., Barnard, J.,
966 Reynolds, W. F., Topol, E. J., DiDonato, J. A., and Hazen, S. L.: Protein
967 carbamylation links inflammation, smoking, uremia and atherogenesis, Nature
968 medicine, 13, 1176-1184, 10.1038/nm1637, 2007.
969 Wang, Z., Yuan, B., Ye, C., Roberts, J., Wisthaler, A., Lin, Y., Li, T., Wu, C., Peng, Y.,
970 Wang, C., Wang, S., Yang, S., Wang, B., Qi, J., Wang, C., Song, W., Hu, W., Wang,
971 X., Xu, W., Ma, N., Kuang, Y., Tao, J., Zhang, Z., Su, H., Cheng, Y., Wang, X., and
972 Shao, M.: High Concentrations of Atmospheric Isocyanic Acid (HNCO) Produced
973 from Secondary Sources in China, Environmental Science & Technology, 54, 11818-
974 11826, 10.1021/acs.est.0c02843, 2020.
975 Wentzell, J. J., Liggio, J., Li, S. M., Vlasenko, A., Staebler, R., Lu, G., Poitras, M. J.,
976 Chan, T., and Brook, J. R.: Measurements of gas phase acids in diesel exhaust: a
977 relevant source of HNCO?, Environmental Science & Technology, 47, 7663-7671,
978 10.1021/es401127j, 2013.
979 Woodward-Massey, R., Taha, Y. M., Moussa, S. G., and Osthoff, H. D.: Comparison of
980 negative-ion proton-transfer with iodide ion chemical ionization mass spectrometry
981 for quantification of isocyanic acid in ambient air, Atmospheric Environment, 98,

982 693-703, 10.1016/j.atmosenv.2014.09.014, 2014.

983 Wren, S. N., Liggio, J., Han, Y., Hayden, K., Lu, G., Mihele, C. M., Mittermeier, R. L.,
984 Stroud, C., Wentzell, J. J. B., and Brook, J. R.: Elucidating real-world vehicle
985 emission factors from mobile measurements over a large metropolitan region: a focus
986 on isocyanic acid, hydrogen cyanide, and black carbon, *Atmospheric Chemistry and
987 Physics*, 18, 16979-17001, 10.5194/acp-18-16979-2018, 2018.

988 Wu, C., Wang, C., Wang, S., Wang, W., Yuan, B., Qi, J., Wang, B., Wang, H., Wang, C.,
989 Song, W., Wang, X., Hu, W., Lou, S., Ye, C., Peng, Y., Wang, Z., Huangfu, Y., Xie,
990 Y., Zhu, M., Zheng, J., Wang, X., Jiang, B., Zhang, Z., and Shao, M.: Measurement
991 report: Important contributions of oxygenated compounds to emissions and
992 chemistry of volatile organic compounds in urban air, *Atmos. Chem. Phys.*, 20,
993 14769-14785, <https://doi.org/10.5194/acp-20-14769-2020>, 2020.

994 Yan, Y., Wang, S., Zhu, J., Guo, Y., Tang, G., Liu, B., An, X., Wang, Y., and Zhou, B.:
995 Vertically increased NO₃ radical in the nocturnal boundary layer, *Science of The
996 Total Environment*, 763, 142969, <https://doi.org/10.1016/j.scitotenv.2020.142969>,
997 2021.

998 Yáñez-Serrano, A. M., Nölscher, A. C., Bourtsoukidis, E., Gomes Alves, E., Ganzeveld,
999 L., Bonn, B., Wolff, S., Sa, M., Yamasoe, M., Williams, J., Andreae, M. O., and
1000 Kesselmeier, J.: Monoterpene chemical speciation in a tropical rainforest: variation
1001 with season, height, and time of day at the Amazon Tall Tower Observatory (ATTO),
1002 *Atmospheric Chemistry and Physics*, 18, 3403-3418, 10.5194/acp-18-3403-2018,
1003 2018.

1004 Yao, L., Wang, M. Y., Wang, X. K., Liu, Y. J., Chen, H. F., Zheng, J., Nie, W., Ding, A.
1005 J., Geng, F. H., Wang, D. F., Chen, J. M., Worsnop, D. R., and Wang, L.: Detection
1006 of atmospheric gaseous amines and amides by a high-resolution time-of-flight
1007 chemical ionization mass spectrometer with protonated ethanol reagent ions,
1008 *Atmospheric Chemistry and Physics*, 16, 14527-14543, 10.5194/acp-16-14527-2016,
1009 2016.

1010 Yu, S.: Role of organic acids (formic, acetic, pyruvic and oxalic) in the formation of
1011 cloud condensation nuclei (CCN): a review, *Atmospheric Research*, 53, 185-217,
1012 [https://doi.org/10.1016/S0169-8095\(00\)00037-5](https://doi.org/10.1016/S0169-8095(00)00037-5), 2000.

1013 Yuan, B., Koss, A. R., Warneke, C., Coggon, M., Sekimoto, K., and de Gouw, J. A.:
1014 Proton-Transfer-Reaction Mass Spectrometry: Applications in Atmospheric Sciences,
1015 *Chemical reviews*, 117, 13187-13229, 10.1021/acs.chemrev.7b00325, 2017.

1016 Yuan, B., Shao, M., de Gouw, J., Parrish, D. D., Lu, S., Wang, M., Zeng, L., Zhang, Q.,
1017 Song, Y., Zhang, J., and Hu, M.: Volatile organic compounds (VOCs) in urban air:
1018 How chemistry affects the interpretation of positive matrix factorization (PMF)
1019 analysis, *Journal of Geophysical Research: Atmospheres*, 117, n/a-n/a,
1020 10.1029/2012jd018236, 2012.

1021 Yuan, B., Veres, P. R., Warneke, C., Roberts, J. M., Gilman, J. B., Koss, A., Edwards,
1022 P. M., Graus, M., Kuster, W. C., Li, S. M., Wild, R. J., Brown, S. S., Dubé, W. P.,
1023 Lerner, B. M., Williams, E. J., Johnson, J. E., Quinn, P. K., Bates, T. S., Lefer, B.,

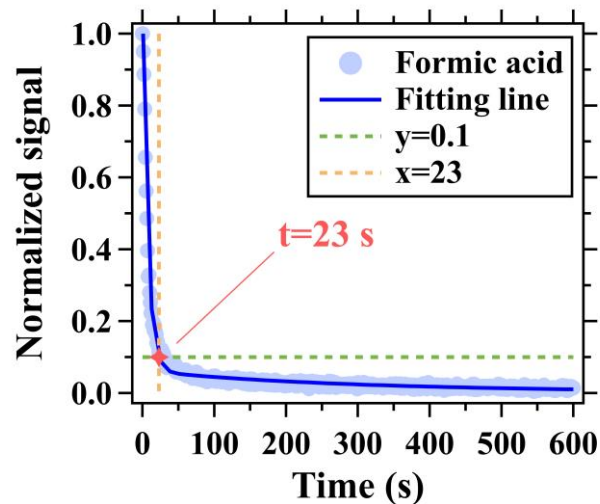
1024 Hayes, P. L., Jimenez, J. L., Weber, R. J., Zamora, R., Ervens, B., Millet, D. B.,
1025 Rappenglück, B., and de Gouw, J. A.: Investigation of secondary formation of formic
1026 acid: urban environment vs. oil and gas producing region, *Atmospheric Chemistry
1027 and Physics*, 15, 1975-1993, 10.5194/acp-15-1975-2015, 2015.

1028 Zhao, R., Yin, B., Zhang, N., Wang, J., Geng, C., Wang, X., Han, B., Li, K., Li, P., Yu,
1029 H., Yang, W., and Bai, Z.: Aircraft-based observation of gaseous pollutants in the
1030 lower troposphere over the Beijing-Tianjin-Hebei region, *Science of The Total
1031 Environment*, 773, 144818, 10.1016/j.scitotenv.2020.144818, 2021.

1032 Zhao, R., Lee, A. K. Y., Wentzell, J. J. B., McDonald, A. M., Toom-Sauntry, D., Leaitch,
1033 W. R., Modini, R. L., Corrigan, A. L., Russell, L. M., Noone, K. J., Schroder, J. C.,
1034 Bertram, A. K., Hawkins, L. N., Abbatt, J. P. D., and Liggio, J.: Cloud partitioning
1035 of isocyanic acid (HNCO) and evidence of secondary source of HNCO in ambient
1036 air, *Geophysical Research Letters*, 41, 6962-6969, 10.1002/2014gl061112, 2014.

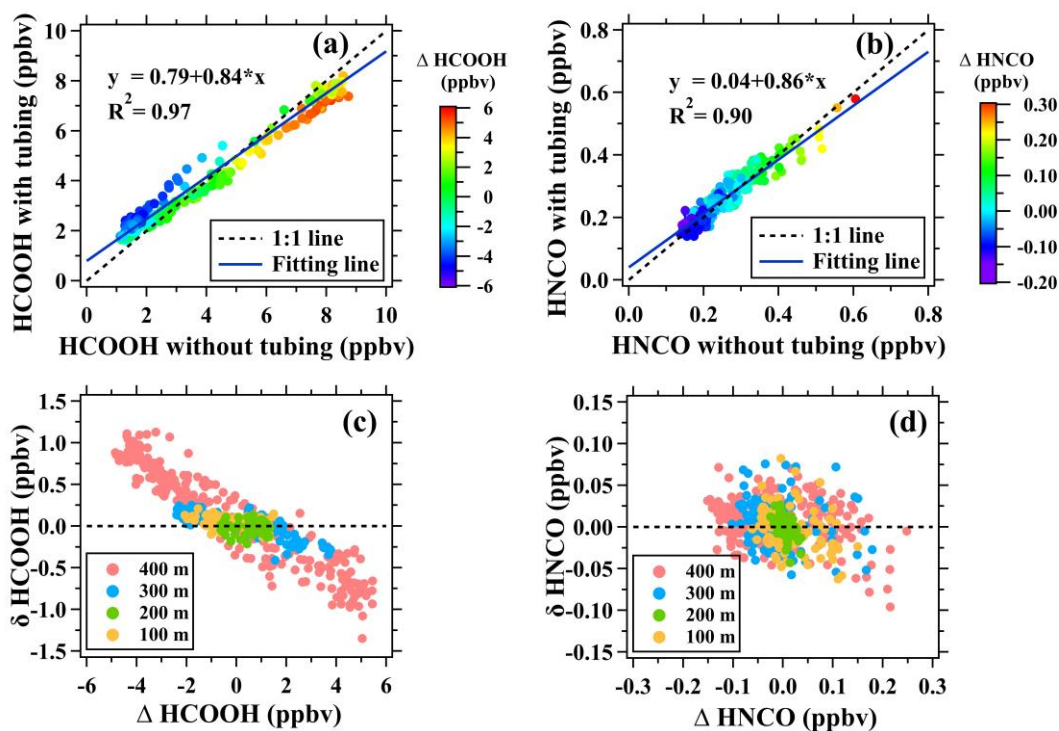
1037 Zhu, B., Han, Y., Wang, C., Huang, X., Xia, S., Niu, Y., Yin, Z., and He, L.:
1038 Understanding primary and secondary sources of ambient oxygenated volatile
1039 organic compounds in Shenzhen utilizing photochemical age-based parameterization
1040 method, *Journal of Environmental Sciences (China)*, 75, 105-114,
1041 10.1016/j.jes.2018.03.008, 2019.

1042



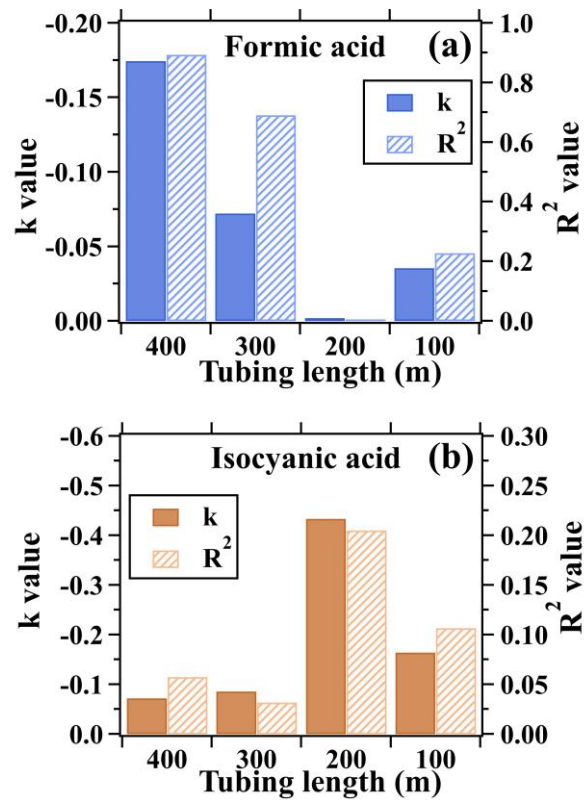
1043

1044 **Figure 1.** Depassivation curves of formic acid signal measured by I^- ToF-CIMS for the
 1045 400 m long tubing at the flow rate of 13 SLPM. Ion signals were normalized to those
 1046 measured at the start time (0 s) of the step-function change.



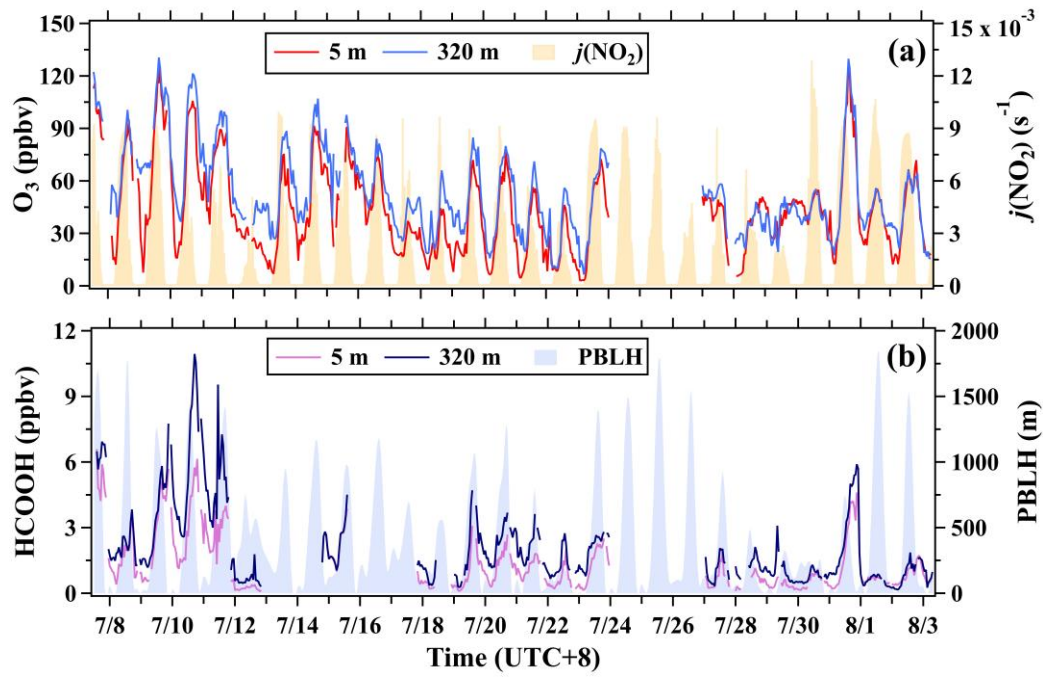
1047

1048 **Figure 2.** Assessment of long tubes in measuring formic and isocyanic acids in ambient
 1049 air. (a-b) Scatterplots of mixing ratios of formic and isocyanic acids measured with the
 1050 400 m long tube versus those measured without the long tube. (c-d) Scatterplots of
 1051 Δ [HCOOH] versus δ [HCOOH] and scatterplots of Δ [HNCO] versus δ [HNCO] for
 1052 the 100, 200, 300, and 400 m tubes.



1053

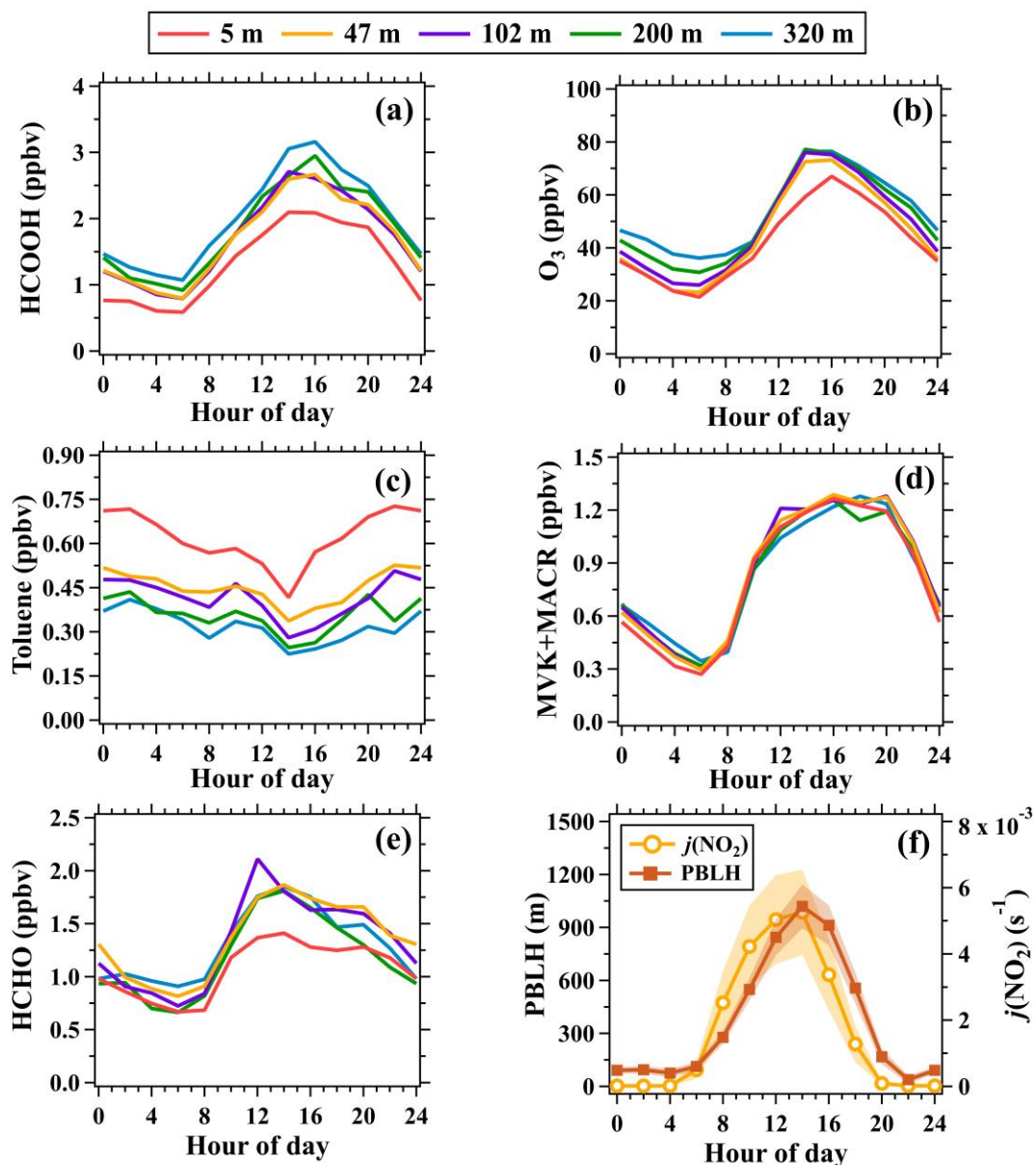
1054 **Figure 3.** Linear fitting parameters (namely k and R^2) for (a) $\Delta[HCOOH]$ versus
 1055 $\delta[HCOOH]$ and (b) $\Delta[HNCO]$ versus $\delta[HNCO]$. The scatterplots are shown in
 1056 Figure 2. k and R^2 are the slope and determination coefficient of the linear fitting lines,
 1057 respectively.



1058

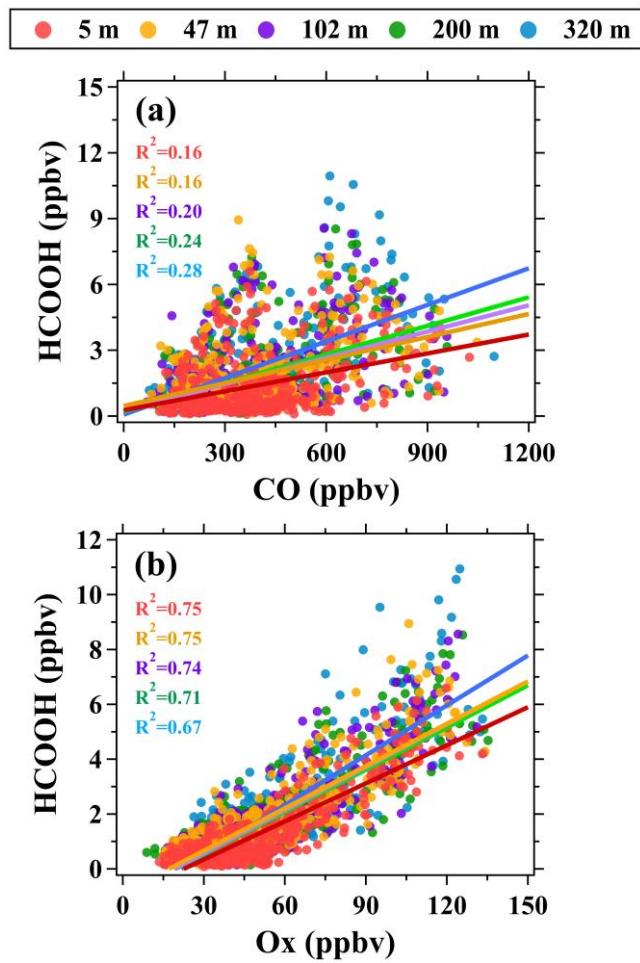
1059 **Figure 4.** Time series of (a) O_3 (5 and 320 m), $j(NO_2)$, (b) formic acid (5 and 320 m),

1060 and planetary boundary layer height (PBLH) during the campaign.



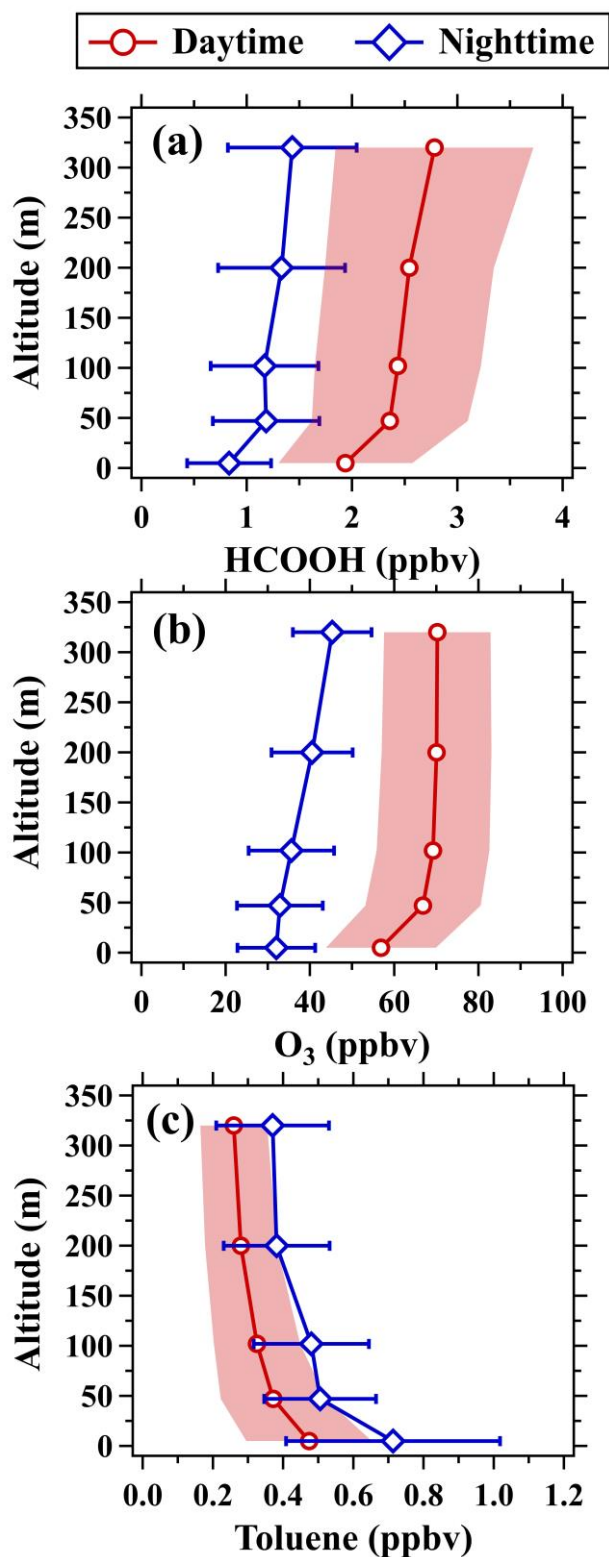
1061

1062 **Figure 5.** Average diurnal variations in mixing ratios of (a) formic acid, (b) O₃, (c)
 1063 toluene, (d) MVK+MACR, (e) formaldehyde at the five inlet heights and (f) PBLH and
 1064 $j(\text{NO}_2)$. The shaded areas in panel (f) are half of the standard deviations.



1065

1066 **Figure 6.** Scatter plots of (a) formic acid versus CO and (b) formic acid versus Ox at
 1067 different altitudes during the campaign.

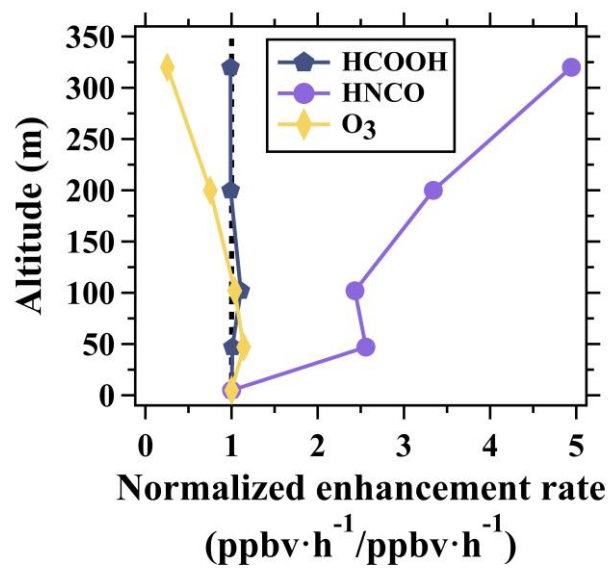


1068

1069 **Figure 7.** Vertical profiles of (a) formic acid, (b) O₃, and (c) toluene in daytime (11:00-

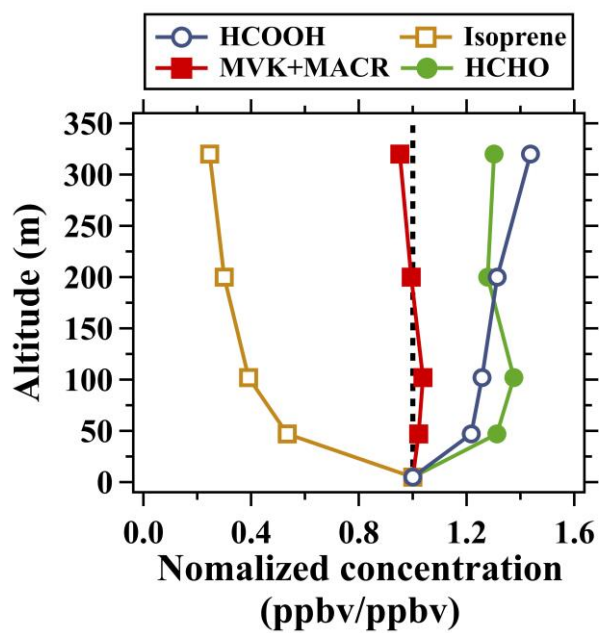
1070 16:00 LT) and nighttime (22:00-5:00 LT). The shaded areas and error bars are half of

1071 the standard deviations.



1072

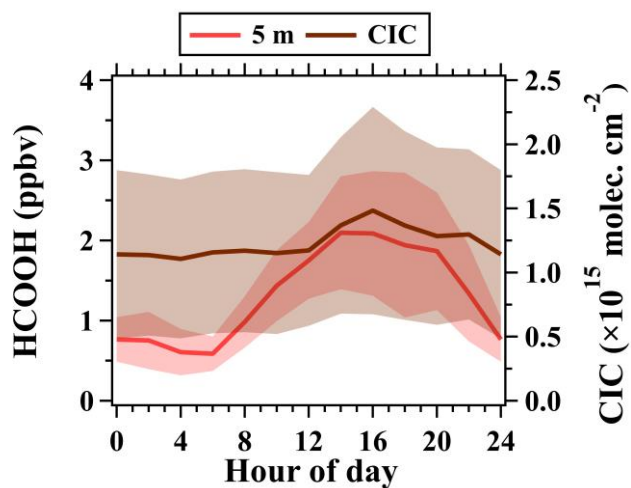
1073 **Figure 8.** Normalized vertical profiles of the enhancement rate of ozone, formic acid,
 1074 and isocyanic acid between 6:00-10:00 LT averaged over the whole campaign.
 1075 Enhancement rate of the species at different altitudes were normalized to those at 5 m.
 1076 The dotted line indicates the normalized enhancement rate of 1.



1077

1078 **Figure 9.** Normalized vertical profiles of formic acid, isoprene, formaldehyde, MVK
 1079 and MACR in daytime (11:00-16:00 LT) averaged over the whole campaign. Mixing
 1080 ratios of the species at different altitudes were normalized to those at 5 m. The dotted
 1081 line indicates the normalized concentration of 1.

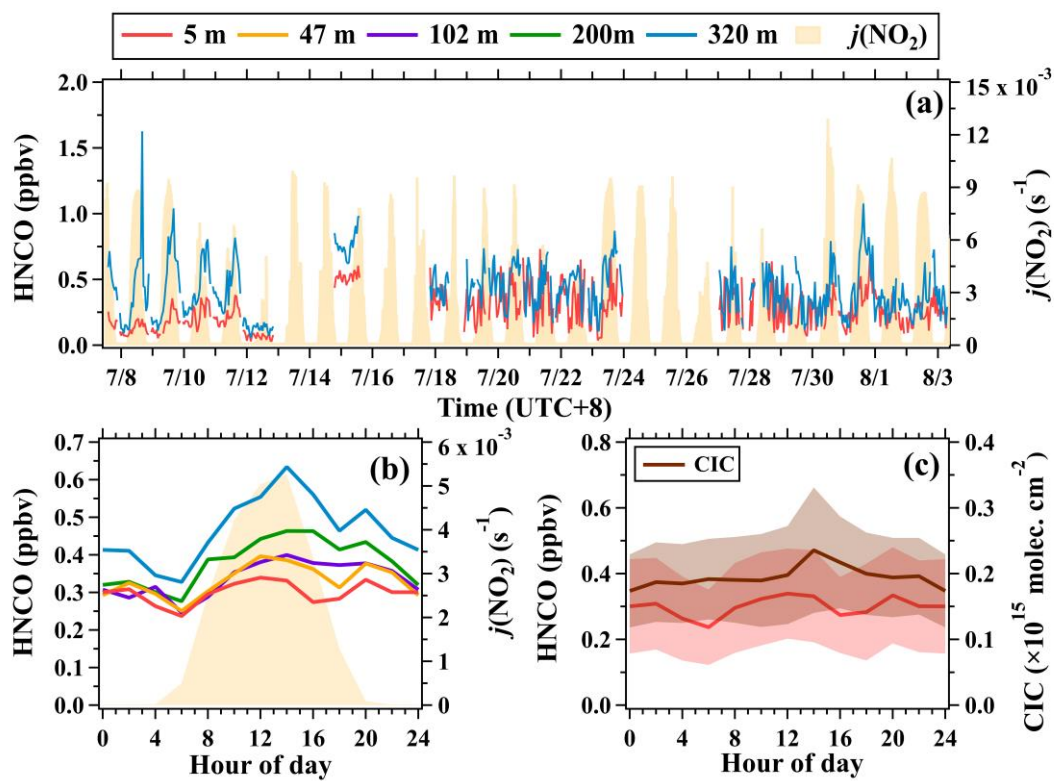
1082



1083

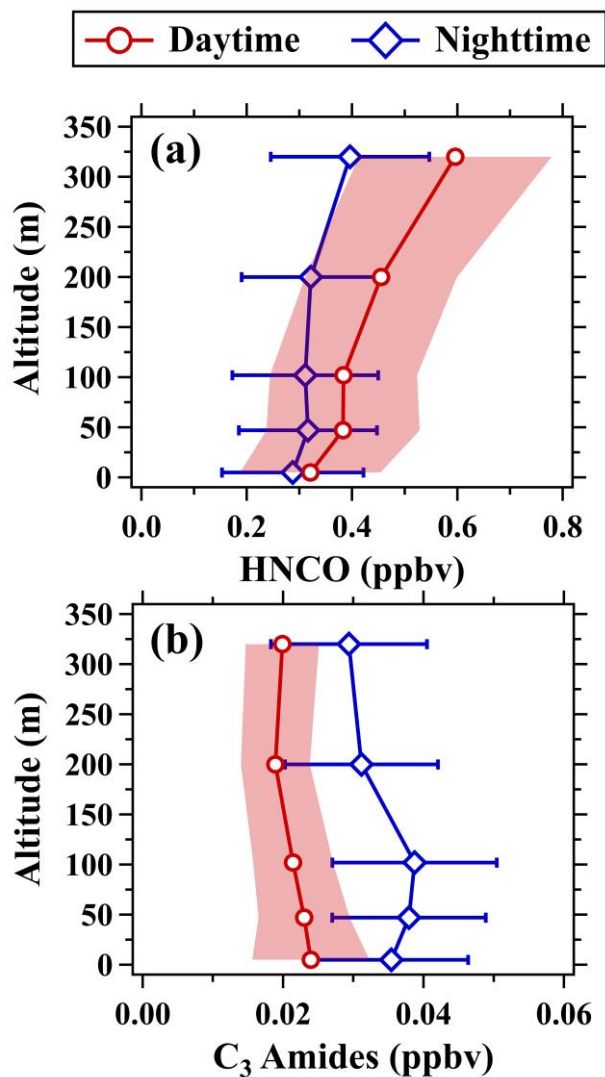
1084 **Figure 10.** Average diurnal variations in mixing ratios (5 m) and CICs of formic acid

1085 during the field campaign; The shaded areas are half of the standard deviations.



1086

1087 **Figure 11.** (a) Time series of isocyanic acid (5 and 320 m) and $j(\text{NO}_2)$. (b) Average
 1088 diurnal variations in isocyanic acid at 5, 47, 102, 200, and 320 m. (c) Average diurnal
 1089 variations in mixing ratios (5 m) and CICs of isocyanic acid during the campaign; The
 1090 shaded areas in panel (c) are half of the standard deviations.



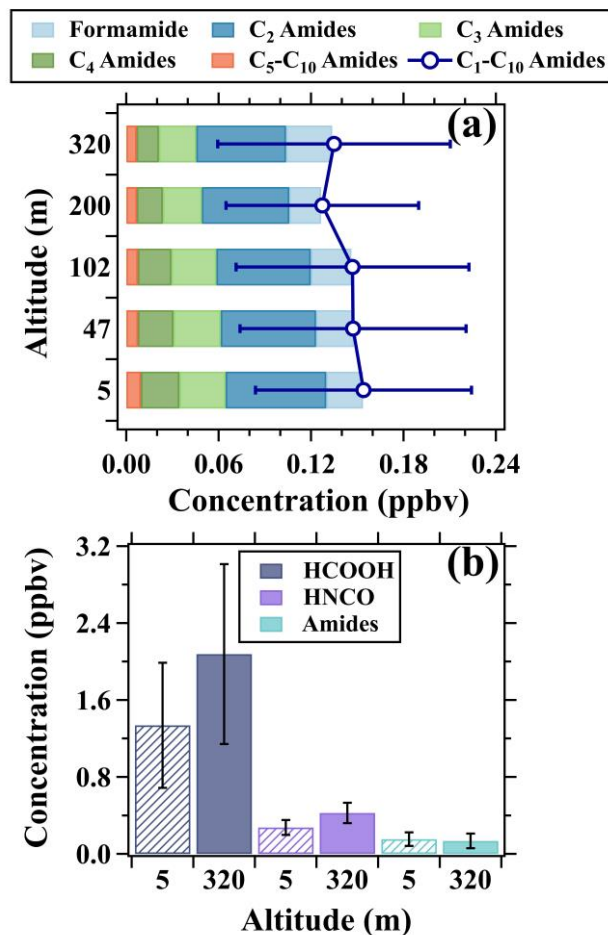
1091

1092 **Figure 12.** Vertical profiles of (a) isocyanic acid and (b) C₃ amides in daytime (11:00-

1093 16:00 LT) and nighttime (22:00-5:00 LT). The shaded areas and error bars are half of

1094 the standard deviations.

1095



1096

1097 **Figure 13.** (a) Vertical variations in composition and concentrations of amides. (b)
 1098 Concentration comparison of formic acid, isocyanic acid, and amides between 5 and
 1099 320 m. The data in both (a) and (b) was the average results of the whole campaign. The
 1100 patterns of the bars are used to distinguish the average concentration of the species at
 1101 the two heights.